# MODELING OF MIXED CONVECTION FOR DOUBLE-PIPE HEAT EXCHANGER IN A PARTIALLY COOLED ENCLOSURE

by

Shuraiya Tasnuva Keya
Student No. 1018092504F
Registration No. 1018092504, Session: October-2018

MASTER OF SCIENCE
IN
MATHEMATICS

Department of Mathematics
BANGLADESH UNIVERSITY OF ENGINEERING AND TECHNOLOGY, DHAKA-1000
August-2021

# CANDIDATE'S DECLARATION

I am hereby declaring that no portion of the work considered in this thesis has been submitted in support of an application for another degree or qualification of this or any other University or Institute of learning either in home or abroad.

_____

**Shuraiya Tasnuva Keya**

August 2021

*In the name of ALLAH, Most Gracious, Most Merciful*

*Dedicated*

*to*

*My Beloved Family*

# ACKNOWLEDGEMENT

All praise is due to Almighty Allah, whose uniqueness, unity and completeness are immutable and without His help no work have been possible.

I would like to express my sincere thanks and gratitude to my esteemed supervisor, Dr. Md. Mustafizur Rahman, Professor, Department of Mathematics, Bangladesh University of Engineering and Technology. I have had a great academic study experience under his supervision and invaluable recommendations and the help has helped me to plan my further academic studies in a better way.

I am grateful from the bottom of my heart to the faculty members of the Department of Mathematics, Bangladesh University of Engineering and Technology especially, to Professor Dr. Khandker Farid Uddin Ahmed, Head, Department of Mathematics, Professor Dr. Md. Manirul Alam Sarker, Professor Dr. Nazma Parveen and all other teachers of this department for their cordial guidance, suggestions and supports. I am also thankful to the external member of the Board of Examiner, Dr. Md. Fazlul Karim, Associate Professor, Mathematical and Physical Sciences, East West University, for his valuable suggestions in improving the quality of my work.

My gratitude goes to the Department of Mathematics, BUET and examinations committee for providing all kinds further logical and organizational supports.

I would like to thank the staff of the Department of Mathematics, Bangladesh University of Engineering and Technology, for their cooperation in this work.

Finally I express my dedicated affection to my family members, my father Md. Shahidur Rahman, who wanted to find me in this position, my mother Anjuman-Ara-Begoum and my younger sister Asma-Ull-Husna Priya, without their cooperation it would be an incomplete task and all other members for creating an comfortable environment in order to complete the courses, research studies and final production of this thesis work.

# ABSTRACT

In this thesis, mixed convection heat transfer for double-pipe heat exchanger in a partially cooled-enclosure has been investigated numerically. The upper lid of the cavity is considered to be moving and a hollow cylinder is used at the middle of the enclosure. Physical problems are governed by the equations of continuity, momentum and energy along with the boundary conditions. The governing equations along with the boundary conditions are transformed into non-dimensional form and solved by employing a finite-element scheme based on the Galerkin weighted residuals method. The investigations are conducted for different governing parameters namely thermal conductivity ratio ($Kr$), Prandtl number ($Pr$), heat generation parameter ($Q$), cooling length ($Lc$), Richardson number ($Ri$), Reynolds number ($Re$). The results are presented in terms of streamlines, isotherms and average heat transfer rate. Computations are done for different values of thermal conductivity ratio $1.1 \leq Kr \leq 30$, Prandtl number $1 \leq Pr \leq 10$, heat generation parameter ratio $0.0 \leq Q \leq 0.75$, cooling length $0.2 \leq Lc \leq 0.8$, Richardson number $0.01 \leq Ri \leq 10$, Reynolds number $50 \leq Re \leq 500$ for different values of dimensionless time ($\tau$) 0.1, 0.5 and 1. The average Nusselt number ($Nu_h$) of the heated surface for different thermal conductivity ratio ($Kr$) shows an oscillatory phenomenon with increasing values of $\tau$. But Prandtl number ($Pr$) increases and heat generation parameter decreases sharply for increasing values of dimensionless time ($\tau$). The other parameters such as cooling length ($Lc$), Richardson number ($Ri$), Reynolds number ($Re$) are not that significant pattern for different values of dimensionless time ($\tau$).

## TABLE OF CONTENTS

# NOMENCLATURE

| | |
|---|---|
| $C_p$ | specific heat at constant pressure ($J/kg.K$) |
| $g$ | gravitational acceleration ($ms^{-2}$) |
| $Gr$ | Grashof number |
| $h$ | convective heat transfer coefficient ($W/m^2.K$) |
| $H$ | height of the cavity ($m$) |
| $Q$ | heat generation parameter |
| $H_\lambda$ | linear shape function |
| $k$ | thermal conductivity of fluid ($Wm^{-1}K^{-1}$) |
| $L$ | length of the cavity ($m$) |
| $n$ | dimensional distance either along $x$ or $y$ direction ($m$) |
| $N$ | non-dimensional distance either along $X$ or $Y$ direction |
| $N_\alpha$ | quadratic shape function |
| $Nu_h$ | Average Nusselt number |
| $p$ | pressure |
| $P$ | non-dimensional pressure |
| $Pr$ | Prandtl number |
| $q_w$ | heat flux |
| $Lc$ | cooling length |
| $Re$ | Reynolds number |
| $Ri$ | Richardson number |
| $Kr$ | thermal conductivity ratio |
| $T$ | dimensional fluid temperature ($K$) |
| $u$ | velocity in $x$-direction ($m/s$) |
| $U$ | dimensionless horizontal velocity |
| $v$ | velocity in $y$-direction ($m/s$) |
| $V$ | dimensionless vertical velocity |
| $x, y$ | Cartesian coordinates ($m$) |
| $X, Y$ | dimensionless Cartesian coordinates |
| $S_x$ | surface tractions along X – axis |
| $S_y$ | surface tractions along Y – axis |
| $k_s$ | thermal conductivity of solid ($Wm^{-1}K^{-1}$) |
| $k_f$ | thermal conductivity of fluid ($Wm^{-1}K^{-1}$) |
| $T_s$ | dimensional solid temperature ($K$) |
| $T_h$ | temperature of the block boundaries |
| $T_w$ | wall temperature |
| $T_\alpha$ | ambient temperature |
| t | dimensional time |

## Greek symbols

| | |
|---|---|
| $\alpha$ | thermal diffusivity ($m^2s^{-1}$) |
| $\beta$ | coefficient of thermal expansion ($K^{-1}$) |
| $\theta$ | dimensionless fluid temperature |
| $\theta_s$ | dimensionless solid temperature |
| $\Delta T$ | dimensionless temperature difference |
| $\mu$ | dynamic viscosity of the fluid ($m^2s^{-1}$) |
| $v$ | kinematic viscosity of the fluid ($m^2s^{-1}$) |
| $\rho$ | density of the fluid ($kgm^{-3}$) |
| $\psi$ | stream function |
| $\pi$ | heat function |
| τ | dimensionless time |
| υ | viscosity |

## Subscripts

| | |
|---|---|
| $h$ | heated wall |
| c | cool wall |
| $s$ | solid |
| $f$ | fluid |
| av | average |

## LIST OF TABLES



## LIST OF FIGURES

# CHAPTER 1

# INTRODUCTION

Modeling is the use of a physical or logical delegation of a given system to create data and help condition or make prophecy about the system. Among many other areas, modeling is extensively used in the manufacturing and product development, social and physical sciences, engineering, among many other areas. Mixed convection is the combination of natural and forced convection flow which is a common occurrence of flow when both external system and internal volumetric forces are determined simultaneously. In the mathematical description of mixed convection in the equations of motion both steps are denoted as the pressure head loss dp/dx and the term for identifying mass forces is retained. Double-pipe heat exchanger in its simplest form, a pipe is centered inside a larger pipe. The inner pipe acts as a conductive barrier where the one liquid flows through this inner pipe and the other flows around it forming an annulus shape with the outer pipe.

## 1.1 HEAT TRANSFER MECHANISM

Heat transfer is the process of transportation of thermal energy from one region to another as a result of temperature difference. Heat can be transferred in three distinct mechanisms or modes: conduction, convection and radiation. A thermal transfer analysis as a system from one unbalanced state to another is related to the amount of heat transfer. The transfer of energy as heat is always from the higher temperature medium to the lower temperature one and heat transfer stops when the two mediums reach the same temperature.

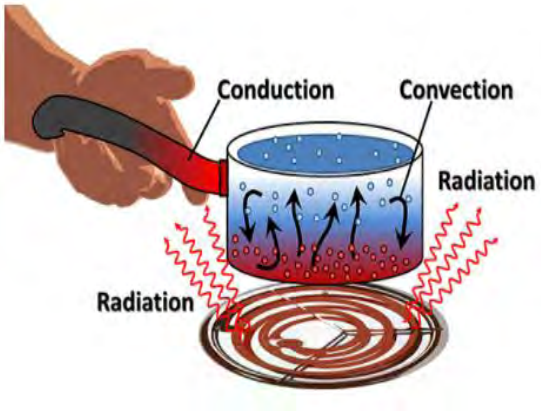


**Figure: 1.1.** Heat transfer mechanism

# Chapter 1

# Chapter 1

# Chapter 1

### 1.2.1 Reynolds Number

In 1883 Osborn Reynolds discovered that the flow regime depends mainly on the inertia forces to viscous forces in the fluid. The Reynolds number (*Re*) is the ratio of inertial force to viscous force within a fluid which is subjected to relative internal movement due to different fluid velocities. Laminar flow occurs at low Reynolds numbers where viscous forces are dominant. Turbulent flow occurs at high Reynolds number and it is dominated by inertial forces which tend to produce chaotic eddies, vortices and other flow instabilities. The transition from laminar to turbulent flow depends on the surface roughness, surface geometry, and surface temperature type of fluid and flow velocity, among other things. This ratio is called the Reynolds number, which is dimensionless quantity and is expressed as

$Re = \rho\, U\, L/\mu$

Where $\rho$, $U$, $L$ and $\mu$ are characteristic values of density, reference velocity, characteristic length and coefficient of viscosity of the fluid flow respectively and $\upsilon = \pi/\rho$ is the kinematics viscosity.

### 1.2.2 Richardson number

The Richardson number (*Ri*) is named after Lewis Fry Richardson (1881-1953). In thermal convection problems, Richardson number represents the importance of natural convection relative to the forced convection. The Richardson number in this context is defined as,

$$Ri = \frac{g\beta\left(T_{hot} - T_{ref}\right)L}{V^2}$$

where $g$ is the gravitational acceleration, $\beta$ is the thermal expansion coefficient, $T_{hot}$ is the hot wall temperature, $T_{ref}$ is the reference temperature, $L$ is the characteristic length and $V$ is the characteristic velocity.

Usually, the forced convection is negligible when $Ri > 10$, the natural convection is negligible when $Ri < 0.1$ and neither is negligible when $0.1 < Ri < 10$.

### 1.2.3 Grashof number

Grashof number is named after Franz Grashof after 28 years of his death. The flow regime in free convection is governed by the dimensionless Grashof number which represents the ratio of the buoyancy force to the viscous forces acting on the fluid.
The Grashof number (*Gr*) is a measure of the relative magnitudes of the buoyancy force acting on the opposing viscous force acting on the fluid.

$$Gr = \frac{g\beta(T_w - T_\alpha)L^3}{v^2}$$

where $g$ is the acceleration due to gravity, $\beta$ is the volumetric thermal expansion coefficient, $T_w$ is the wall temperature, $T_\alpha$ is the ambient temperature, $L$ is the characteristic length and $\nu$ is the kinematics viscosity. The role played by the Grashof number in free convection is played by the Reynolds number in forced convection. As such, the Grashof number provides the main criterion in determining whether the fluid flow is laminar or turbulent in natural convection.

### 1.2.4 Prandtl number

In 1904, Ludwig Prandtl introduced the concept of boundary layer and made significant contributions to boundary layer theory.
The Prandtl number is a non-dimensional number according to the name of the Garman physicist Ludwig Prandtl defined as the ratio of the speed of thermal insulation. In heat transfer problems, the Prandtl number controls the velocity and the relative thickness of the thermal boundary layers. The Schmidt number is the mass transfer analog of the Prandtl number. When *Pr* is small, it means that the heat dissipates faster than the velocity. This means that the thickness of the thermal boundary layer for liquid metals is much larger than the velocity boundary layer. Small values of the Prandtl number, $Pr \ll 1$, means the thermal diffusivity dominates. Whereas with large values, $Pr \gg 1$, the momentum diffusivity dominates the behavior. In heat transfer problems, the Prandtl number controls the relative thickness of the momentum and thermal boundary layers. When *Pr* is small, it means that the heat diffuses quickly compared to the velocity (momentum). This means that for liquid metals the thermal boundary layer is much thicker than the velocity boundary layer.

The relative thickness of the velocity and the thermal boundary layers is best described by the dimensionless parameter Prandtl number, define as,

$$Pr = \frac{Viscous\ diffusion\ rate}{Thermal\ diffusion\ rate}$$
$$= \frac{\nu}{\alpha}$$
$$= \frac{\mu c_p}{k}$$

For liquid metals, the Prandtl number of fluid range is less than 0.01 which is more than 100000 for heavy oils. For water, the Prandtl number is in the order of 7 and for air is 0.71. Air at room temperature has a Prandtl number of 0.71 and for water at $18^0$ C it is around 7.56, which means that the thermal diffusivity is more dominant for air than for water. For many fluids, *Pr* lies in the range from 1 to 10. For gases, *Pr* is generally about 0.7. For liquid metals the Prandtl number is very small, generally in the range from 0.01 to 0.001. This means that the thermal diffusivity, which is related to the rate of heat transfer by conduction, unambiguously dominates.

## 1.3 DOUBLE-PIPE HEAT EXCHANGER

Heat exchangers are a basic tool throughout every industry and for good reason. These devices can transfer or exchange heat between two flows (liquid or gas) via a conductive barrier without physical mixing. This heat is a kind of energy and engineers have created a system where heat exchangers are used to efficiently transfer energy between paths. A pipe centered inside a large pipe which is called double-pipe. Double-pipe heat exchanger is one of the simplest forms. The inner pipe acts as a conductive barrier where a liquid flows through this inner pipe. Another stream flows around it forming an annulus shape with the outer pipe. The outside flow passes over the inside flow which will cause heat exchanger through the inner tube's wall. Double-pipe heat exchangers can be categorized based on the flow direction. Parallel flow and counter flow can be deployed in these exchanges and it is all about the position of inlets and outlets. The best design for double pipe heat exchangers is counter flow. In this pattern, the heat exchanger has the optimum heat transfer coefficient and can cold or heats the outlets as we desire. Parallel flow is the type that the inlets and outlets are in one head. Heat transfer is less than the counter

# Chapter 1

## 1.4 PARTIALLY COOLED ENCLOSURE

Guimaraes and Menon [17] has investigated a two-dimensional natural convection with a protuberant heat source and non-steady regime that may resemble an electrical transformer in a square partially cooled enclosure. A steady of non-Darcy natural convection in a square cavity due to the partially cooled sidewalls enclosure filled with heat generating medium has been numerically investigated by Wu et al. [41]. In a lid-driven enclosure, numerical simulation of magnetohydrodynamic mixed convection with a constant flux heater for fluid flow and heat transfer has been analyzed by Ogut [34]. Natural convection problem inside a square enclosure to solve the two-dimensional equations for steady state finite element method is used by Chowdhury et al. [11]. They found that the average Nusselt number decrease with the increasing value of block size for partially heated and cooled square enclosure. Rahman et al. [37] has used finite element method to solve the unsteady natural convection heat transfer and fluid flow through double-pipe with a hollow cylinder in a partially cooled enclosure. They found that the length and position would not have a serious change on natural convection for low Rayleigh number. When the partial cooler is situated in the middle of the vertical wall than the maximum heat transfer is created.

## 1.5 APPLICATION

Mixed convection heat transfer has always been a great interest of the researchers because of its wide applications in different engineering sectors and many industrial areas such as building and thermal insulation system, the cooling systems of electronic devices, the food storage industry, the numerical reactor system, solar collectors, float glass production, chemical processing equipment, the geophysical fluid mechanics, drying technologies etc.

## 1.6 LITERATURE REVIEW

A numerical study on mixed convection flow in a square lid driven cavity is important for both theoretical and practical points of view. The effect of mixed convection flows in cavities; channels are investigated by many researchers by using

numerical, analytical and experimental methods. Such a problem is grouped under lid driven cavity. Some essential works are presented below.

Keeping upper and bottom walls are thermally insulated and left and right walls are lid-driven the steady state two-dimensional mixed convection problem with heated square cavity has been numerically investigated by Oztop and Dagtekin [29]. Containing a temperature gradient of two-dimensional flow in a two sided lid-driven cavity was investigated by Luo and Yang [22]. Heat radiation transferred into a square cavity by mixed convection taking the upper horizontal wall is lid-driven has been investigated numerically by Belmiloud and Chemloul [4]. In their study, they found that the influence of angles and its variety of Richardson number on the change of the average Nusselt number. Laminar mixed convection flow of a radiating gas in a bended lid-driven cavity where the fluid treated as a dispersion, gray, throw and drying medium is studied by Addini and Nassab [1]. Steady state mixed convection for three dimensional in a lid-driven cubical cavity heating from below where the vertical walls are thermally insulated has been investigated numerically by Mansour et al. [24]. Using commercial finite volume package FLUENT, a steady laminar mixed convection flow and heat transfer in a lid-driven cavity for the computational fluid dynamics model has been studied by Omari [33]. Steady mixed convection under the combined buoyancy effects of thermal and mass diffusion in a square lid-driven cavity by Galerkin wighted residual method using several parameters for heat and mass transfer rate was examined numerically by Al-Amiri et al. [2]. Two dimensional laminar mixed convection heat transfers with shallow rectangular driven cavities, where top moving lid is at a higher temperature of aspect ratio 10 was studied numerically by Sharif [39]. Unsteady laminar mixed convection heat transfer forced convection flow inside a lid-driven cavity is attained by a mechanically induced sliding lid as it is set to oscillate horizontally in a sinusoidal currency has been numerically investigated by Khanafer et al. [20]. Heat Transfer mechanisms and flow characteristics depend on Reynolds numbers, Grashof numbers and the number of undulations for mixed convection flow and heat transfer in a lid-driven cavity with wavy bottom surface which was performed by Saha et al. [38]. Mixed convection in a lid-driven cavity with arc-shaped moving wall was considered numerically by Ismael [18]. In the presence of partial slip, the heat transfer rate

increases with the Richardson number for steady mixed convection in a lid-driven cavity which is filled with water was investigated by Ismael et al. [19]. The flow field and the temperature distribution are influenced by Prandtl number on mixed convection in a lid-driven cavity was considered by Moallemi and Jang [23]. The numerical simulation of the effects of inclination angle, Richardson number and aspect ratio on the flow of structure and heat transfer in air inside two-dimensional cavity where the flow was induced by a shear force caused by a cooled upper moving lid with the buoyancy from bottom heating was performed by Cheng and Liu [10]. Considering different shapes of hot bottom wall in a lid driven cavity for mixed convection has been examined by Yapici and Obut [42]. Laminar natural convection in an enclosure with finite thickness and conductivity divided by a partition has been studied by Kahveci [21].

Having a circular body a study of fluid flow due to combined convection in lid-driven enclosure has been investigated by Oztop et al. [30]. An adiabatic block inside a lid-driven cavity probably put down the energy circulation to enhance thermal energy transport has been studied by Biswas et al. [5]. With the presence of an endothermic obstacle inside an inclined square lid-driven cavity resulting from synchronous mixed convection natural and forced heat transfer has been numerically simulated and investigated by Balootaki et al. [7]. Laminar mixed convection in two-dimensional lid-driven cavity with constant flux and internal elliptic heat source on the bottom wall was numerically studied by Munshi et al. [25]. The effect of hydromagnetic mixed convection heat transfer to a two-dimensional alloy the internal elliptical heated block is conveyed in a double lid-driven square cavity is studied numerically by Munshi and Alim [26]. The increasing value of Hartman number reduced the heat transfer in a lid-driven square cavity with a corner heater for mixed convection heat transfer was reported by Oztop et al. [30]. Heat transfer and mixed convection flow in a shallow enclosure with a series of block-like heat generating components for a range of block-to-fluid thermal conductivity ratios and Grashof numbers and Reynolds numbers was studied numerically by Bhoite et al. [8]. For mixed convection flow the effect of Reynolds number with heat generating obstacle in a lid- driven cavity was investigated by Parvin et al. [35]. Mixed convection in the lid-driven cavity with internal heating barriers in different places

the inclination angles of the cavity with the new formation of the variable properties were studied by Esfe et al. [13]. Using finite volume method a two-dimensional vertical lid-driven cavity of convection flow and heat transfer inclined elliptical obstacle with joule heating has been numerically investigated by Deb et al. [12].

Using finite difference method for different parameters to investigate the effect of mixed convection of MHD flow and partially heated wavy walled lid-driven enclosure, this computational work has been done by Oztop et al. [31]. Keeping left and right vertical walls are constant temperature in a lid driven cavity having a heated circular hollow cylinder sited at the center of the cavity with magneto-hydrodynamic mixed convection is studied numerically by Farid et al. [15]. By finite volume method and SIMPLE algorithm, keeping bottom wall cold, top moving lid wall is kept hot temperature and vertical walls are well insulated the effects of magnetic field gravity on fluid flow and heat transfer in a square lid-driven cavity is analyzed by Bakar et al. [6]. Around a heat conducting horizontal circular cylinder along with joule heating a numerical study of magnetohydrodynamic mixed convection has been carried out by Rahman et al. [36]. In that study, it was found that the result of streamlines, isotherms, average Nusselt number, average fluid temperature and dimensionless temperature depend on Richardson number, Hartmann number and the cavity aspect ratio. Filled with water-CuO nanofluid a steady laminar mixed convection flow in a lid-driven cavity with wavy wall in numerical model are investigated by Nada and Chamkha [28]. They found that the presence of nanoparticles increases the significance of the thermal transfer increase for all values of the Richardson number and geometry ratio of the bottom wall. In the presence of a magnetic field a problem of unsteady laminar combined convection flow and heat transfer in a vertical lid-driven cavity of an electrically heat generating and conducting or absorbing fluid was numerically investigated by Chamkha [9]. In the presence of magnetic field on a lid-driven mixed convection square cavity when both vertical side walls are partially heated and cooled has been analyzed by Sivasankaran et al. [40]. The two-dimensional mixed convection flow in a lid-driven cavity using the pseudo spectral method based on polyharmonic spline radial basis functions in the presence of partial magnetic field has been investigated by Geridonmez and Oztop [16]. Using Lattice Boltzmann method in the presence of

cubic obstacle in a square lid-driven cavity for mixed convection flow utilizing nanofluid was investigated by Afrouzi and Farhadi [3]. A comparative study of mixed convection flow in a two-dimensional lid driven square cavity filled with Cu-water nanofluid has been investigated by Malik and Nayak [27]. Numerical solution of mixed convection in filled cavities for nanofluid field was investigated by Esfe et al. [14].

## 1.7 MOTIVATION

It is clear from the above literature review, that there are ample scope less attention has been given to study of mixed convection for double-pipe heat exchanger. However, the study of mixed convection for double-pipe heat exchanger is important for numerous engineering applications. The analysis of the effect of mixed convection flow for different shapes and different boundary conditions to ensure efficient performance of heat transfer equipment's. For solar collectors, nuclear reactor, micro electrical equipment and many other problems mixed convection heat exchanger is very important. On the other side, the maximum work of the mixed convection heat exchanger has been carried out cavity or channel. In recent years many scientists and researchers have started to show their interest in the study of mixed convection for double-pipe heat exchanger in a partially cooled enclosure. To observe the variation in heat transfer and fluid flow, numerical analysis are essential and this is the basis for the motivation behind the present study.

## 1.8 OBJECTIVES

Research on mixed convection introduced flow is increasingly interested in many engineering applications, for examples in heat exchangers, transport of heated or cooled fluids, microelectronic cooling and so on. From the literature survey mentioned above, it is observed that less attention has been given to study mixed convection for double-pipe heat exchanger. The study carried out numerically with an accurate numerical procedure and the related results will be shown using streamlines, isotherms and related graphs and charts. The specific objectives of the present research work are:

- To derive the mathematical model with regard to the proposed study.

- To find numerical solution of the developed model.
- To investigate the effects of pertinent parameters namely Prandtl number, Reynolds number, Richardson number, Nusselt number and the effects of physical parameters namely solid fluid conductivity ratio and length of cooling source on the flow and thermal fields in the enclosure.
- To compare the present result with related published result.

## 1.9 OUTLINE OF THE THESIS

This thesis paper contains four chapters. In chapter 1, a brief introduction is presented with aim and objective. This chapter also consists of a literature review of the past studies on fluid flow and heat transfer in cavities or channels. There are many cavity configurations for the study of conjugate effect of conduction and mixed convection. In this study we have considered a square lid driven cavity.

In Chapter 2, mathematical model along with the computational procedure of the problem has been presented.

In Chapter 3, a detailed results and discussion is directed.

Finally, in Chapter 4, the main achievements and some ideas of further work have been summarized.

# CHAPTER 2

## MATHEMATICAL MODELLING

The mathematical model describes a system that uses mathematical concepts and language. The process of developing a mathematical model is called mathematical modeling. Mathematical models are used in the natural sciences (such as physics, chemistry, biology, earth sciences) and in engineering disciplines (such as computer sciences, electrical engineering) as well as in non-physical systems such as social sciences, sociology, psychology, political sciences. Mathematical models can take many forms including dynamic systems, statistical models, differential equations or game theoretical models. In many cases, the quality of the scientific field depends on how well the mathematically developed models agree with the results of the repetitive experiments. In physical sciences, a traditional theoretical mathematical model consists mostly of the following elements:

1) Governing equations
2) Supplementary sub-models
    a. Defining equations
    b. Constitutive equations
3) Assumptions and constraints
    a. Initial and boundary conditions
    b. Classical constraints and kinematic equations

Often engineers use mathematical models when analyzing to control or optimize a system. In the analysis engineers can create a descriptive model of the system as an estimate of how the system might work or try to estimate how an unexpected event could affect the system. Similarly, in controlling a system engineers can try different control methods in simulation. A mathematical model typically describes a system by establishing a relationship between a variable and a set of equations. Variables can be different types, real or integer numbers, Boolean values or strings for example.

Mathematical models are a necessary part of the simulation and design of control systems. The purpose of the mathematical model is to provide a simple representative of reality, mimicking the relevant features of the systems analysis. There are two main categories of mathematical modeling: theoretical and experimental modeling.

In theoretical modeling, the system is described using equations derived from physics. In order to be able to model the system in such a way, several simplifications have to be applied. For example, when modeling the suspension of a vehicle, we assume that the stiffness of the spring is constant, even if in reality is not. Experimental modeling, also called system identification, is based on measurements**.** The mathematical model of the system is derived from several sets of measurements, each recording the system's response (output) for different stimulus and perturbations (inputs).

The finite element method (FEM) is one of the numerical methods that have received popularity due to its capability for solving complex problems. Finite element method is used to solve the non-dimensional governing equations along with boundary conditions for the considered problem. In this study, FEM is applied for discretization of the governing equations. It is assumed that the incoming fluid in the cavity is two dimensional viscous and incompressible. The solution of the governing equations along with the boundary conditions is obtained through the Galerkin finite element formulation. Then investigation involving each term of these equations is performed by using Gauss's quadrature method.

The numerical procedure used in this work is based on the Galerkin weighted residual method of finite element formulation. The application of this technique is described well by Taylor- Hood (1973) and Dechaumphai (1999). In their method, the solution domain has been discretized into finite element meshes, which are composed of non-uniform triangular elements. Then the nonlinear governing partial differential equations (i.e. mass, momentum and energy equations) has been transferred into a system of integral equations by applying Galerkin weighted residual method. Using Gauss quadrature method, performs the integration involved in each term of these equations. The nonlinear algebraic equations so obtained are modified by imposition of boundary conditions. These modified nonlinear equations

are transferred into linear algebraic equations using Newton's method and then solve these linear equations using Triangular Factorization method. Finally, parametric results are presented in terms of streamlines, isotherms, average Nusselt number at the heated surface and average temperature of the fluid in the cavity. The post-processing results of the system are used to predict the flow and rate of heat transfer through the heat exchanger.

The remainder of this chapter is as follows. In section 2.1, the physical configurations of the current research interest are shown. Then the appropriate mathematical model (both governing equations and boundary conditions) is considered in section 2.2. After that, a numerical scheme that is employed in this study is described in the section 2.3.

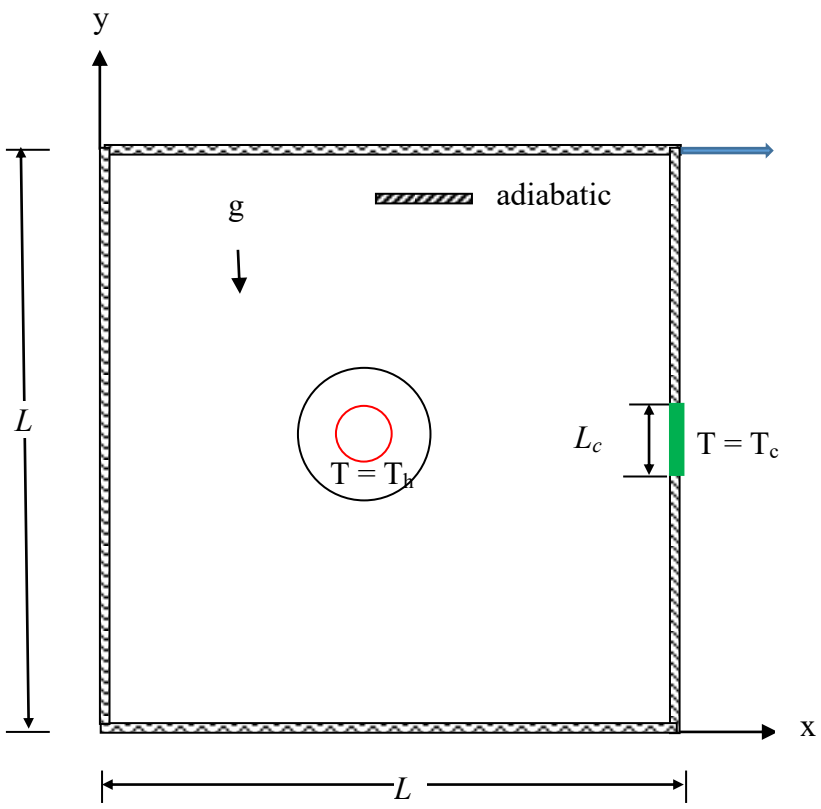


**Figure: 2.1.** Schematic diagram for the problem with boundary conditions and coordinate system

## 2.1 PHYSICAL MODEL

The schematic of the problem herein investigated is presented in the figure 2.1. The system consists of a lid-driven square cavity enclosure with $L$ length. The both left and right walls of the enclosure are kept adiabatic and the right wall of the enclosure

is partially cooled. Length of partial cooler is depicted by *Lc*. Gravity acts in vertical direction. The upper wall of the enclosure is lid-driven. Heated part of the heat exchanger has a constant hot temperature due to hot fluid inside the inner cylinder. The diameter of inner and outer tube is taken as constant for whole study. Outer part of hollow cylinder is filled by air with Prandtl number.

## 2.2 GOVERNING EQUATIONS ALONG WITH BOUNDARY CONDITIONS

The fundamental laws used to solve the heat transfer and fluid flow problems are the conservation of mass (continuity equations), momentum equations and energy equations. It constitutes a set of nonlinear, coupled and partial differential equations. In the $\nu$-momentum equation, the buoyancy force is included here as a body force for laminar incompressible thermal flow. The governing equations for the two-dimensional steady flow after involving the Boussinesq approximation and neglecting radiation and viscous dissipation can be expressed as

Continuity Equation

$$\frac{\partial u}{\partial x} + \frac{\partial v}{\partial y} = 0 \tag{2.1}$$

Momentum Equations

$$\frac{\partial u}{\partial t} + u\frac{\partial u}{\partial x} + v\frac{\partial u}{\partial y} = -\frac{1}{\rho}\frac{\partial p}{\partial x} + \upsilon\left(\frac{\partial^2 u}{\partial x^2} + \frac{\partial^2 u}{\partial y^2}\right) \tag{2.2}$$

$$\frac{\partial v}{\partial t} + u\frac{\partial v}{\partial x} + v\frac{\partial v}{\partial y} = -\frac{1}{\rho}\frac{\partial p}{\partial y} + \upsilon\left(\frac{\partial^2 v}{\partial x^2} + \frac{\partial^2 v}{\partial y^2}\right) + g\beta(T - T_c) \tag{2.3}$$

Energy Equations

$$\frac{\partial T}{\partial t} + u\frac{\partial T}{\partial x} + v\frac{\partial T}{\partial y} = \frac{k}{\rho c_p}\left(\frac{\partial^2 T}{\partial x^2} + \frac{\partial^2 T}{\partial y^2}\right) \tag{2.4}$$

For solid block, $\frac{k_s}{\rho c_p}\left(\frac{\partial^2 T_s}{\partial t^2} + \frac{\partial^2 T_s}{\partial x^2} + \frac{\partial^2 T_s}{\partial y^2}\right) + q = 0$ (2.5)

where, $q$ is the heat flux per unit volume and $x$ and $y$ are the distances measured along the horizontal and vertical directions respectively; $u$ and $v$ are the velocity components in the $x$ and $y$ directions respectively; $T$ and $T_s$ denote the fluid and solid temperature respectively, $T_c$ denotes the reference temperature for which buoyant

force vanishes, $p$ is the pressure, $\rho$ is the density, $g$ is the gravitational force, $\beta$ is the volumetric coefficient of thermal expansion, $c_p$ is the fluid specific heat, $k$ and $k_s$ are the thermal conductivity of fluid and solid respectively.

**Boundary conditions**

The dimensional boundary conditions under consideration can be written as:

For $t = 0$: $u = v = 0, T = 0, p = 0$

For $t > 0$:

At the upper lid: $u = U_0, v = 0, \frac{\partial T}{\partial n} = 0$

At the left wall: $u = 0, v = 0, \frac{\partial T}{\partial n} = 0$

At the right wall: $u = 0, v = 0, T = 0$ at cooled part and $\frac{\partial T}{\partial n} = 0$ at the remaining part

At the outer surface of the hollow cylinder: $\begin{cases} u = 0, v = 0 \\ \left(\frac{\partial T}{\partial n}\right)_{fluid} = K\left(\frac{\partial T_s}{\partial n}\right)_{solid} \end{cases}$

At the inner surface of the hollow cylinder: u $= 0, v = 0, T = T_h$

where, $n$ is the non-dimensional distances either along $x$ or $y$ direction acting normal to the surface and $Kr = k_s / k_f$ is the thermal conductivity of the fluid.

The average Nusselt number at the heated surface of the cylinder based on the dimensional quantities may be expressed by

$Nu_h = -\frac{2}{\pi}\int_0^{\pi}\frac{\partial T}{\partial n}ds$

The average Nusselt number can be used in process engineering design calculations to estimate the rate transfer from the heated surface.

**Dimensional analysis**

Non-dimensional variables are used for making the governing equations (2.1−2.5) into dimensionless form are stated as follows:

$$X = \frac{x}{L}, Y = \frac{y}{L}, U = \frac{u}{u_0}, V = \frac{v}{u_0}, D = \frac{d}{L}, P = \frac{p}{\rho {u_0}^2}, \tau = \frac{tv}{L^2}\ \theta = \frac{T - T_c}{T_h - T_c},$$

$$\theta_s = \frac{T_s - T_c}{T_h - T_c}$$

where, $X$ and $Y$ are the coordinates varying along horizontal and vertical directions, respectively, $U$ and $V$ are the velocity components in the $X$ and $Y$ directions, respectively, $\theta$ is the dimensionless temperature and $P$ is the dimensionless pressure. After substitution the dimensionless variables into the equations (2.1-2.5), we get the following dimensionless equations as

Continuity Equation

$$\frac{\partial U}{\partial X} + \frac{\partial V}{\partial Y} = 0 \tag{2.6}$$

Momentum Equations

$$\frac{\partial U}{\partial \tau} + U\frac{\partial U}{\partial X} + V\frac{\partial U}{\partial Y} = -\frac{\partial P}{\partial X} + \frac{1}{Re}\left(\frac{\partial^2 U}{\partial X^2} + \frac{\partial^2 U}{\partial Y^2}\right) \tag{2.7}$$

$$\frac{\partial V}{\partial \tau} + U\frac{\partial V}{\partial X} + V\frac{\partial V}{\partial Y} = -\frac{\partial P}{\partial Y} + \frac{1}{Re}\left(\frac{\partial^2 V}{\partial X^2} + \frac{\partial^2 V}{\partial Y^2}\right) + Ri\theta \tag{2.8}$$

Energy Equations

$$\frac{\partial \theta}{\partial \tau} + U\frac{\partial \theta}{\partial X} + V\frac{\partial \theta}{\partial Y} = \frac{1}{RePr}\left(\frac{\partial^2 \theta}{\partial X^2} + \frac{\partial^2 \theta}{\partial Y^2}\right) \tag{2.9}$$

For solid block, $\frac{K}{RePr}\left(\frac{\partial^2 \theta_s}{\partial \tau^2} + \frac{\partial^2 \theta_s}{\partial X^2} + \frac{\partial^2 \theta_s}{\partial Y^2}\right) + Q = 0$ (2.10)

The dimensionless parameters appearing in the equations (2.6) through (2.10) are the Reynolds number *Re*, Prandtl number *Pr*, Grashof number *Gr,* Richardson number *Ri* and solid fluid thermal conductivity ratio *K*. They are respectively defined as follows:

$$Re = \frac{UL}{\upsilon}, Gr = \frac{g\beta\Delta T L^3}{\upsilon^2}, Ri = \frac{Gr}{Re^2}, Q = \frac{qL^2}{k_s \Delta T}, K_r = \frac{k_s}{k_f}$$

where, $\Delta T = T_h - T_c$ and $\alpha = \frac{k}{\rho c_p}$ are the temperature difference and thermal diffusivity of the fluid respectively.

The dimensionless boundary conditions under consideration can be written as:

For $\tau = 0$: $U = V = 0$, $\theta = 0$, $P = 0$

For $\tau > 0$:

At the upper lid: $U = 1,\ V = 0,\ \frac{\partial \theta}{\partial N} = 0$

At the left wall: $U = 0,\ V = 0,\ \frac{\partial \theta}{\partial N} = 0$

At the right wall: $U = 0,\ V = 0,\ \theta = 0$ at cooled part and $\frac{\partial \theta}{\partial N} = 0$ at the remaining part

At the outer surface of the hollow cylinder: $\begin{cases} U = 0, V = 0 \\ \left(\frac{\partial \theta}{\partial N}\right)_{fluid} = K\left(\frac{\partial \theta_s}{\partial N}\right)_{solid} \end{cases}$

At the inner surface of the hollow cylinder: $U = 0,\ V = 0,\ \theta = 1$

Here $N$ is the non-dimensional distances along $X$ and $Y$ direction acting normal to the surface and $Kr = k_s\ k_f$ is the solid fluid thermal conductivity ratio.

The average Nusselt number at the heated surface of the cylinder based on the dimensionless quantities may be expressed by $Nu_h = -\frac{2}{\pi}\int_0^{\pi} \frac{\partial \theta}{\partial N} ds$. The stream function is calculated from its definition as, $U = \frac{\partial \psi}{\partial Y}, V = -\frac{\partial \psi}{\partial X}$

## 2.3 NUMERICAL ANALYSIS

The governing equations along with the boundary conditions are solved numerically, employing Galerkin weighted residual finite element techniques discussed below.

### 2.3.1 FINITE ELEMENT FORMULATION AND COMPUTATIONAL PROCEDURE

To derive the finite element equations, the method of weighted residuals Zienkiewicz and Taylor (1991) is applied to the equations (2.6) – (2.10) as

$$\int_A N_\alpha \left(\frac{\partial U}{\partial X} + \frac{\partial V}{\partial Y}\right) dA = 0 \tag{2.11}$$

$$\int_A N_\alpha \left(\frac{\partial U}{\partial \tau} + U\frac{\partial U}{\partial X} + V\frac{\partial V}{\partial Y}\right) dA = -\int_A H_\lambda \left(\frac{\partial P}{\partial X}\right) dA + \frac{1}{Re}\int_A N_\alpha \left(\frac{\partial^2 U}{\partial X^2} + \frac{\partial^2 V}{\partial Y^2}\right) dA \tag{2.12}$$

$$\int_A N_\alpha \left(\frac{\partial V}{\partial \tau} + U\frac{\partial V}{\partial X} + V\frac{\partial V}{\partial Y}\right) dA = -\int_A H_\lambda \left(\frac{\partial P}{\partial Y}\right) dA + \frac{1}{Re}\int_A N_\alpha \left(\frac{\partial^2 V}{\partial X^2} + \frac{\partial^2 V}{\partial Y^2}\right) dA + Ri\int_A N_\alpha T dA \tag{2.13}$$

$$\int_A N_\alpha \left(\frac{\partial \theta}{\partial \tau} + U\frac{\partial \theta}{\partial X} + V\frac{\partial \theta}{\partial Y}\right) dA = \frac{1}{RePr}\int_A N_\alpha \left(\frac{\partial^2 \theta}{\partial X^2} + \frac{\partial^2 \theta}{\partial Y^2}\right) dA \quad (2.14)$$

$$\frac{K}{RePr}\int_A N_\alpha \left(\frac{\partial^2 \theta_s}{\partial \tau^2} + \frac{\partial^2 \theta_s}{\partial X^2} + \frac{\partial^2 \theta_s}{\partial Y^2}\right) dA + Q = 0 \quad (2.15)$$

where, $A$ is the element area, $N_\alpha$ ($\alpha$ = 1, 2, …… , 6) are the element interpolation functions for the velocity components and the temperature, and $H_\lambda$ ($\lambda$ = 1, 2, 3) are the element interpolation functions for the pressure.

Gauss's theorem is then applied to equations (2.12)-(2.15) to generate the boundary integral terms associated with the surface tractions and heat flux. Then equations (2.12)-(2.15) become,

$$\int_A N_\alpha \left(\frac{\partial U}{\partial \tau} + U\frac{\partial U}{\partial X} + V\frac{\partial U}{\partial Y}\right) dA + \int_A H_\lambda \left(\frac{\partial P}{\partial X}\right) dA + \frac{1}{Re}\int_A \left(\frac{\partial N_\alpha}{\partial X}\frac{\partial U}{\partial X} + \frac{\partial N_\alpha}{\partial Y}\frac{\partial U}{\partial Y}\right) dA = \int_{S_0} N_\alpha S_x dS_0 \quad (2.16)$$

$$\int_A N_\alpha \left(\frac{\partial V}{\partial \tau} + U\frac{\partial V}{\partial X} + V\frac{\partial V}{\partial Y}\right) dA + \int_A H_\lambda \left(\frac{\partial P}{\partial Y}\right) dA + \frac{1}{Re}\int_A \left(\frac{\partial N_\alpha}{\partial X}\frac{\partial V}{\partial X} + \frac{\partial N_\alpha}{\partial Y}\frac{\partial V}{\partial Y}\right) dA - Ri\int_A N_\alpha \theta dA = \int_{S_0} N_\alpha S_y dS_0 \quad (2.17)$$

$$\int_A N_\alpha \left(\frac{\partial \theta}{\partial \tau} + U\frac{\partial \theta}{\partial X} + V\frac{\partial \theta}{\partial Y}\right) dA + \frac{1}{RePr}\int_A \left(\frac{\partial N_\alpha}{\partial X}\frac{\partial \theta}{\partial X} + \frac{\partial N_\alpha}{\partial Y}\frac{\partial \theta}{\partial Y}\right) dA = \int_{S_w} N_\alpha q_{1w} dS_w \quad (2.18)$$

$$\frac{K}{RePr}\int_A \left(\frac{\partial N_\alpha}{\partial \tau}\frac{\partial \theta_s}{\partial \tau} + \frac{\partial N_\alpha}{\partial X}\frac{\partial \theta_s}{\partial X} + \frac{\partial N_\alpha}{\partial Y}\frac{\partial \theta_s}{\partial Y}\right) dA = \int_{S_w} N_\alpha q_{2w} dS_w \quad (2.19)$$

Here (2.16)-(2.17) specifying surface tractions ($S_x$, $S_y$) along outflow boundary $S_0$ and (2.18)-(2.19) specifying velocity components and fluid temperature or heat flux ($q_w$) that flows into or out from domain along wall boundary $S_w$.

The basic unknowns for the above differential equations are the velocity components $U$, $V$ the temperature, $\theta$ and the pressure, $P$. The six node triangular element is used in this work for the development of the finite element equations. All six nodes are associated with velocities as well as temperature; only the corner nodes are associated with pressure. This means that a lower order polynomial is chosen for pressure and which is satisfied through continuity equation. The velocity component and the temperature distributions and linear interpolation for the pressure distribution

according to their highest derivative orders in the differential equations (2.6)-(2.10) as

$$U(X,Y) = N_\beta U_\beta \tag{2.20}$$

$$V(X,Y) = N_\beta V_\beta \tag{2.21}$$

$$\theta(X,Y) = N_\beta \theta_\beta \tag{2.22}$$

$$\theta_s(X,Y) = N_\beta \theta_{s\beta} \tag{2.23}$$

$$P(X,Y) = H_\lambda P_\lambda \tag{2.24}$$

where $\beta = 1, 2, \ldots\ldots, 6$; $\lambda = 1, 2, 3$.

Substituting the element velocity component distributions, the temperature distribution, and the pressure distribution from equations (2.20)-(2.24), the finite element equations can be written in the form,

$$K_{\alpha\beta^x} U_\beta + K_{\alpha\beta^y} V_\beta = 0 \tag{2.25}$$

$$K_{\alpha\beta}\dot{U}_\beta + K_{\alpha\beta\gamma^x} U_\beta U_\gamma + K_{\alpha\beta\gamma^y} V_\gamma U_\gamma + M_{\alpha\mu^x} P_\mu + \frac{1}{Re}\left(S_{\alpha\beta^{xx}} + S_{\alpha\beta^{yy}}\right)U_\beta = Q_{\alpha^u} \tag{2.26}$$

$$K_{\alpha\beta}\dot{V}_\beta + K_{\alpha\beta\gamma^x} U_\beta V_\gamma + K_{\alpha\beta\gamma^y} V_\gamma V_\gamma + M_{\alpha\mu^y} P_\mu + \frac{1}{Re}\left(S_{\alpha\beta^{xx}} + S_{\alpha\beta^{yy}}\right)V_\beta - RiK_{\alpha\beta}\theta_\beta = Q_{\alpha^v} \tag{2.27}$$

$$K_{\alpha\beta}\dot{\theta}_\beta + K_{\alpha\beta\gamma^x} U_\beta \theta_\gamma + K_{\alpha\beta\gamma^y} V_\beta \theta_\gamma + \frac{1}{RePr}\left(S_{\alpha\beta^{xx}} + S_{\alpha\beta^{yy}}\right)\theta_\beta = Q_{\alpha^\theta} \tag{2.28}$$

$$\frac{K}{RePr}\left(S_{\alpha\beta^{\tau\tau}} + S_{\alpha\beta^{xx}} + S_{\alpha\beta^{yy}}\right)\theta_\beta = Q_{\alpha^{\theta_s}} \tag{2.29}$$

Where superposed dot denotes partial differentiation with respect to $\tau$ and the coefficients in element matrices are in the form of the integrals over the element area and along the element edges $S_0$ and $S_w$ as

$$K_{\alpha\beta^x} = \int_A N_\alpha N_{\beta,x} dA \tag{2.30a}$$

$$K_{\alpha\beta^y} = \int_A N_\alpha N_{\beta,y} dA \tag{2.30b}$$

$$K_{\alpha\beta\gamma^x} = \int_A N_\alpha N_\beta N_{\gamma,x} dA \tag{2.30c}$$

$$K_{\alpha\beta\gamma^y} = \int_A N_\alpha N_\beta N_{\gamma,y} dA \tag{2.30d}$$

$$K_{\alpha\beta} = \int_A N_\alpha N_\beta dA \tag{2.30e}$$

$$S_{\alpha\beta^{xx}} = \int_A N_{\alpha,x} N_{\beta,x} dA \tag{2.30f}$$

$$S_{\alpha\beta^{yy}} = \int_A N_{\alpha,y} N_{\beta,y} dA \tag{2.30g}$$

$$M_{\alpha\mu^x} = \int_A H_\alpha H_{\mu,x} dA \tag{2.30h}$$

$$M_{\alpha\mu^y} = \int_A H_\alpha H_{\mu,y} dA \tag{2.30i}$$

$$Q_{\alpha^u} = \int_{S_0} N_\alpha S_x dS_0 \tag{2.30j}$$

$$Q_{\alpha^v} = \int_{S_0} N_\alpha S_y dS_0 \tag{2.30k}$$

$$Q_{\alpha^\theta} = \int_{S_w} N_\alpha q_{1w} dS_w \tag{2.30$l$}$$

$$Q_{\alpha^{\theta_s}} = \int_{S_w} N_\alpha q_{2w} dS_w \tag{2.30m}$$

These element matrices are evaluated in closed form ready for numerical simulation. Details of the derivation for these element matrices are omitted herein.

The derived finite element equations (2.25)-(2.29) are nonlinear. These nonlinear algebraic equations are solved by applying the Newton-Raphson iteration technique by first writing the unbalanced values from the set of the finite element equations (2.25)-(2.29) as,

$$F_{\alpha^p} = K_{\alpha\beta^x} U_\beta + K_{\alpha\beta^y} V_\beta \tag{2.31a}$$

$$F_{\alpha^u} = K_{\alpha\beta} \dot{U}_\beta + K_{\alpha\beta\gamma^x} U_\beta U_\gamma + K_{\alpha\beta\gamma^y} V_\gamma U_\gamma + M_{\alpha\mu^x} P_\mu + \frac{1}{Re}\left(S_{\alpha\beta^{xx}} + S_{\alpha\beta^{yy}}\right) U_\beta - Q_{\alpha^u} \tag{2.31b}$$

$$F_{\alpha^v} = K_{\alpha\beta} \dot{V}_\beta + K_{\alpha\beta\gamma^x} U_\beta V_\gamma + K_{\alpha\beta\gamma^y} V_\gamma V_\gamma + M_{\alpha\mu^y} P_\mu + \frac{1}{Re}\left(S_{\alpha\beta^{xx}} + S_{\alpha\beta^{yy}}\right) V_\beta - RiK_{\alpha\beta}\theta_\beta - Q_{\alpha^v} \tag{2.31c}$$

$$F_{\alpha^\theta} = K_{\alpha\beta}\dot{\theta}_\beta K_{\alpha\beta\gamma^x} U_\beta \theta_\gamma + K_{\alpha\beta\gamma^y} V_\beta \theta_\gamma + \frac{1}{RePr}\left(S_{\alpha\beta^{xx}} + S_{\alpha\beta^{yy}}\right)\theta_\beta - Q_{\alpha^\theta} \tag{2.31d}$$

$$F_{\alpha^{\theta_s}} = \frac{K}{RePr}\left(S_{\alpha\beta^{\tau\tau}} + S_{\alpha\beta^{xx}} + S_{\alpha\beta^{yy}}\right)\theta_{s\beta} - Q_{\alpha^{\theta_s}} \tag{2.31e}$$

This leads to a set of algebraic equations with the incremental unknowns of the element nodal velocity components, temperatures, and pressures in the form,

$$\begin{bmatrix} K_{pu} & K_{pv} & 0 & 0 & 0 \\ K_{uu} & K_{uv} & 0 & K_{up} & 0 \\ K_{\theta u} & K_{\theta v} & K_{\theta\theta} & 0 & 0 \\ K_{vu} & K_{vv} & K_{v\theta} & K_{vp} & 0 \\ 0 & 0 & 0 & 0 & K_{\theta_s\theta_S} \end{bmatrix} \begin{Bmatrix} \Delta p \\ \Delta u \\ \Delta\theta \\ \Delta v \\ \Delta\theta_s \end{Bmatrix} = -\begin{Bmatrix} F_{\alpha^p} \\ F_{\alpha^u} \\ F_{\alpha^\theta} \\ F_{\alpha^v} \\ F_{\alpha^{\theta_s}} \end{Bmatrix} \tag{2.32}$$

Where $K_{uu} = K_{\alpha\beta}\dot{U}_\beta + K_{\alpha\beta\gamma^x}U_\beta + K_{\alpha\gamma\beta^x}U_\gamma + K_{\alpha\beta\gamma^y}V_\beta + \frac{1}{Re}(S_{\alpha\beta^{xx}} + S_{\alpha\beta^{yy}})$

$K_{uv} = K_{\alpha\beta\gamma^u}U_\gamma$

$K_{u\theta} = K_{u\theta_s} = 0, K_{up} = M_{\alpha\mu^x}, K_{vu} = K_{\alpha\beta\gamma^x}V_\gamma$

$K_{vv} = K_{\alpha\beta}\dot{V}_\beta + K_{\alpha\beta\gamma^x}U_\beta + K_{\alpha\gamma\beta^x}V_\gamma + K_{\alpha\beta\gamma^y}V_\gamma + \frac{1}{Re}(S_{\alpha\beta^{xx}} + S_{\alpha\beta^{yy}})$

$K_{v\theta} = -RiK_{\alpha\beta}, K_{vp} = M_{\alpha\mu^\gamma}$

$K_{\theta u} = K_{\alpha\beta\gamma^x}\theta_\gamma, K_{\theta v} = K_{\alpha\beta\gamma^y}\theta_\gamma, K_{v\theta_s} = 0$

$K_{\theta\theta} = K_{\alpha\beta}\dot{\theta}_\beta + K_{\alpha\beta\gamma^x}U_\beta + K_{\alpha\beta\gamma^y}V_\beta + \frac{1}{RePr}(S_{\alpha\beta^{xx}} + S_{\alpha\beta^{yy}}), K_{\theta p} = K_{\theta\theta_s} = 0, K_{\theta_s u} = K_{\theta_s v} = K_{\theta_s\theta} = K_{\theta_s p} = 0$

The iteration process is terminated if the percentage of the overall change compared to the previous iteration is less than the specified value.

To solve the sets of the global nonlinear algebraic equations in the form of matrix, the Newton-Raphson iteration technique has been adapted through PDE solver with MATLAB interface. The convergence of solutions is assumed when the relative error for each variable between consecutive iterations is recorded below the convergence criterion ε such that $|\psi^{n+1} - \psi^n| < \varepsilon$, where n is number of iteration and $\psi = U, V, \theta$. The convergence criterion was set $\varepsilon = 10^{-5}$.

### 2.3.2 GRID SIZE SENSITIVITY TEST

A lid-driven cavity is considered as the geometry in this chapter. Therefore several grid size sensitivity test are conducted in the geometry to determine the sufficiency of the mesh scheme and to ensure that the solutions are grid dependent. In order to solve non-linear residual equations with the boundary conditions mentioned earlier, the average Nusselt numbers for various non-uniform grids of triangular elements: 2654, 4674, 5936, 6102 and 7574 are offered to build up an understanding of the grid

excellence that is essential for perfect numerical solution as seen in figure 2.2. There is considerable change in the average Nusselt number from 2654 to 5936 and no noticeable change is found from 5936 to 7574. Hence taking into account the correctness of the results obligatory and computational time concerned the elements 5936 is chosen for all computational job.

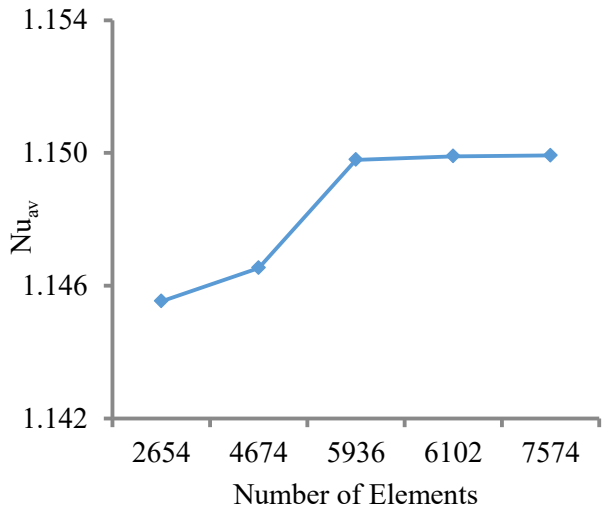


**Figure: 2.2.** Grid independency study for $Re$ = 100, $Ri$ = 1, $Pr$ = 0.71, $Kr$ = 5.3, $Q$ = 0.2, $Lc$ = 0.3.

### 2.3.3 VALIDATION OF THE NUMERICAL SCHEME

It is important to compare the results with the previously published results to verify the accuracy of the numerical results and the validity of the mathematical models obtained throughout the present study. The present numerical code is validated against two published research. First one is the problem of laminar natural convection in an enclosure with finite thickness and conductivity which is separated by a partition studied by Kahveci (2007). The enclosure is heated using an equal heat flow over the vertical wall and cooled to a constant temperature on the opposite wall.

The comparison of the calculated average Nusselt number using the present numerical code for $Ra = 10^6$, $Xp = 0.5$, $w = 0.1$ and $K = 0.001$ with the published work done by Kahveci (2007). Comparatively good agreement is found as shown in Table 2.1.

**Table 2.1.** Comparison of average Nusselt number between present study and Kahveci (2007)

| Kahveci (2007) | | Present work | |
|---|---|---|---|
| Partition wall | Cold wall | Partition wall | Cold wall |
| 1.63 | 1.94 | 1.65 | 1.93 |

Second research, which we validated in our study is done by Oztop et al. (2009) who studied mixed convection heat transfer in a lid driven cavity having a circular body. The comparison between present work and Oztop et al. (2009) for streamlines and isotherms at different diameter (a) $D = 0.3L$, (b) $D = 0.4L$, and (c) $D = 0.5L$ are presented in the Figure 2.3 and 2.4 respectively. This can be seen from the figures that the present work and those reported work in Oztop et al. (2009) are in excellent agreement.

We are, therefore, confident that the results reported in our paper are accurate. Finally, this validity increases confidence in numerical results of current work.

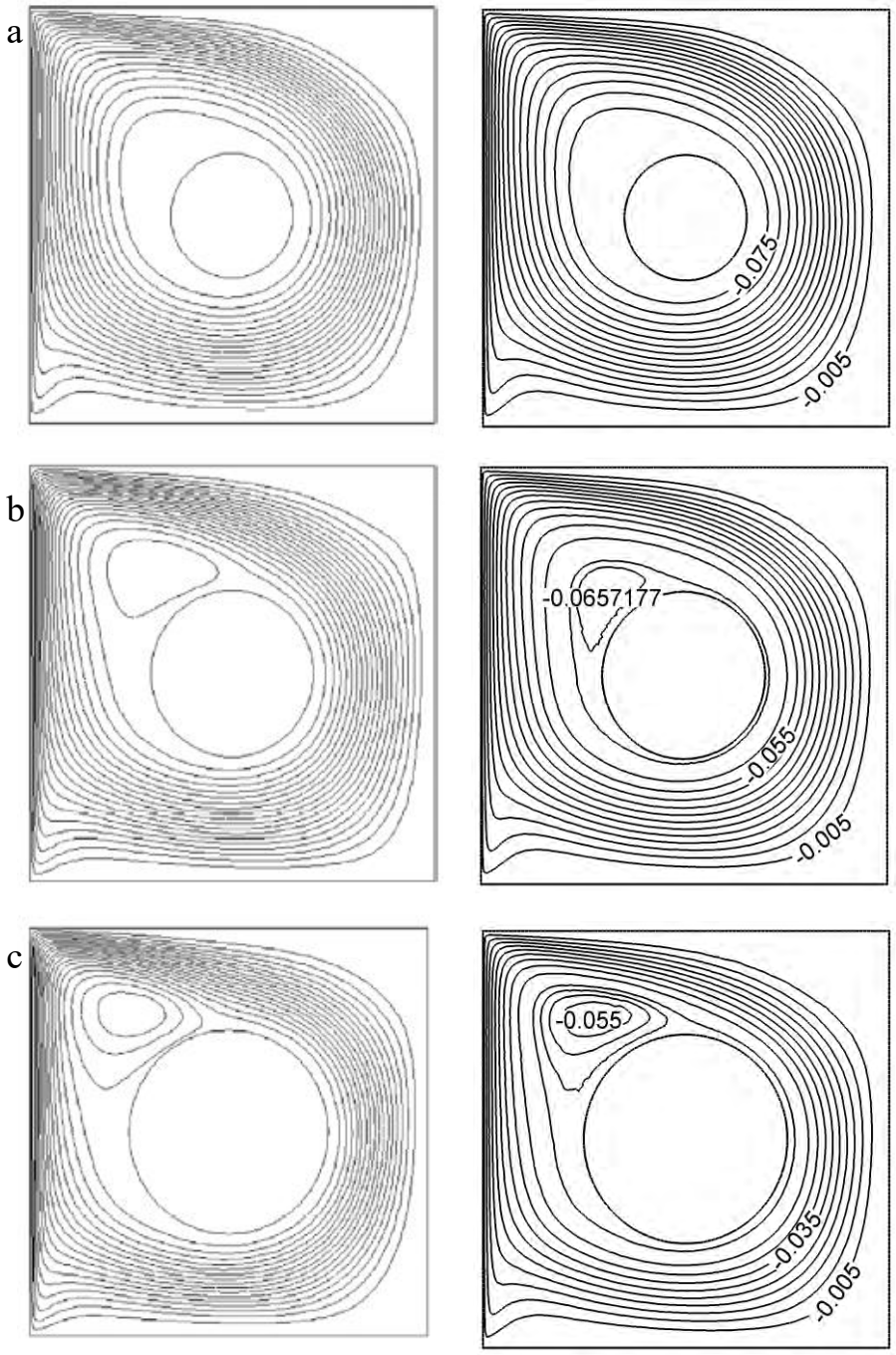


**Figure: 2.3.** Comparison of the streamlines between the present work (right) and that of Oztop et al. (2009) (left) at different diameter (a) $D = 0.3L$, (b) $D = 0.4L$ and (c) $D = 0.5L$.

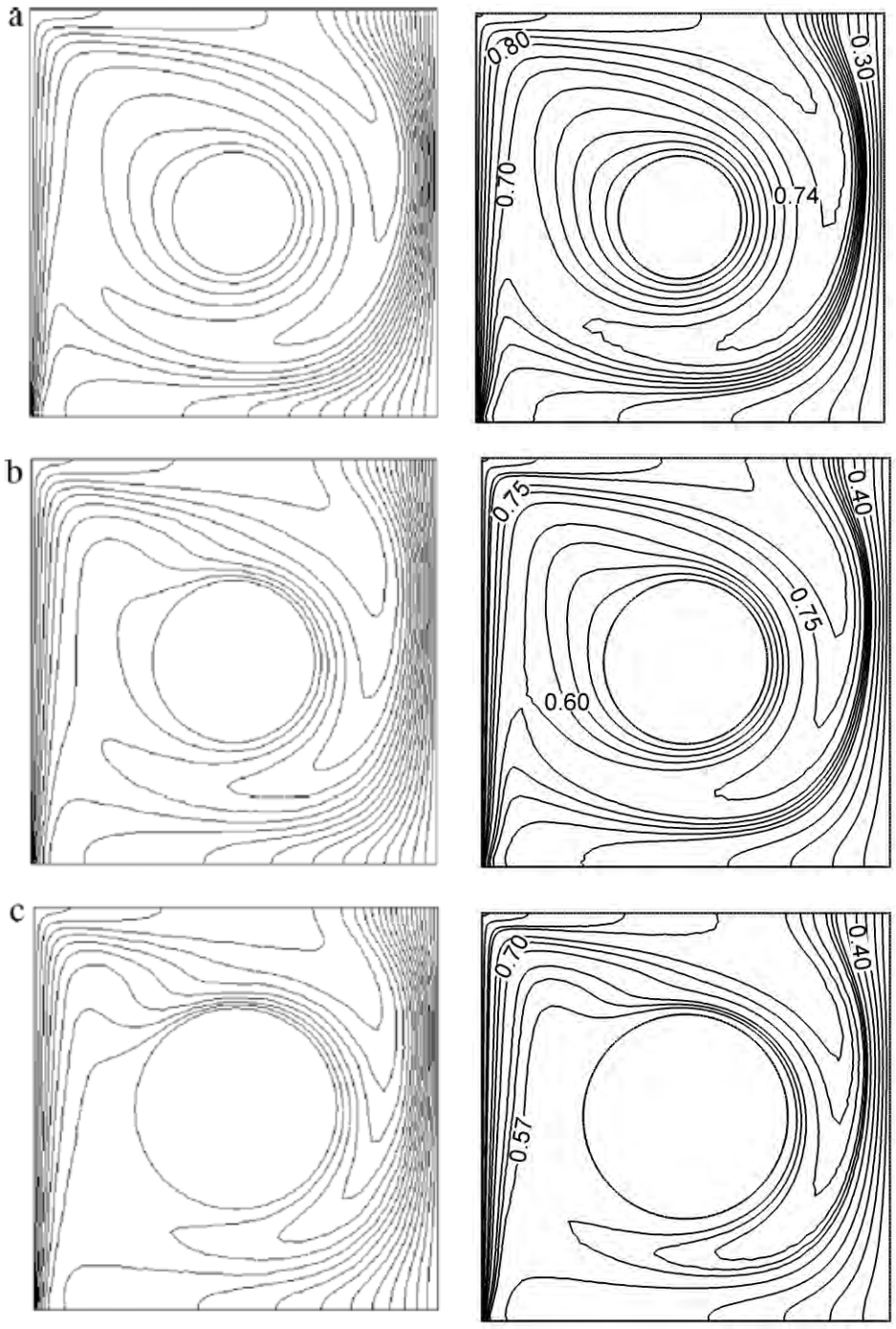


**Figure: 2.4.** Comparison of the isotherms between the present work (right) and that of Oztop et al. (2009) (left) at different diameter (a) $D = 0.3L$, (b) $D = 0.4L$ and (c) $D = 0.5L$.

# CHAPTER 3

## RESULTS AND DISCUSSION

The present numerical study is carried out for mixed convection heat transfer for double pipe heat exchanger with the help of finite – element method. The current investigation is to explore the conjugate effect of mixed convection heat transfer in a square cavity in the presence of heat generating object. Numerical results are presented in order to determine the effects of the dimensionless parameters. The dimensionless parameters that must be specified for the system are solid fluid thermal conductivity ratio (*Kr*), Prandtl number (*Pr*), heat generating parameter (*Q*), cooling length (*Lc*), Richardson number (*Ri*) and Reynolds number (*Re*). The values of the solid fluid thermal conductivity ratio varies from 1 to 30, Prandtl number varies from 1 to 10, heat generation parameter varies from 0 to 0.75, cooling length varies from 0.2 to 0.8, Richardson number varies from 0.01 to 10, Reynolds number varies from 50 to 500. The results are presented in terms of streamline and isotherms patterns. The variations of the average heat transfer rate are also highlighted.

### 3.1 EFFECT OF THERMAL CONDUCTIVITY RATIO

The effect of solid-fluid thermal conductivity ratio (*Kr*) on flow field while *Re* = 100, *Pr* = 0.71, *Q* = 0.2, *Ri* = 1, *Lc* = 0.3 at dimensionless time ($\tau$) 0.1, 0.5, 1 are displayed in the column of the figure 3.1 and 3.2. The results are presented in terms of streamlines and isotherms pattern. Figure 3.1 is showing the streamlines for different values of thermal conductivity ratio *Kr* from 1.1 to 30. Here, the color indicates the temperature of flow field, blue is for lower temperature and red color indicates higher temperature. Here, some maximum and minimum values for different values of thermal conductivity ratio are obtained. When, *Kr* = 30 and $\tau$ = 0.1 and 1, then the maximum values and minimum values are very closer. When *Kr* = 1.1 and $\tau$ = 0.1 the minimum value is near the upper boundary and maximum value is near the right boundary. For $\tau$ = 0.5 number of cells are equal for all values of *Kr* except *Kr* = 1.1. When *Kr* = 3.3 and $\tau$ = 0.5 the minimum value is very close to the hollow cylinder. At high thermal conductivity ratio the mixed convection plays a dominant role and the recirculation flow is mostly generated by the moving lid.

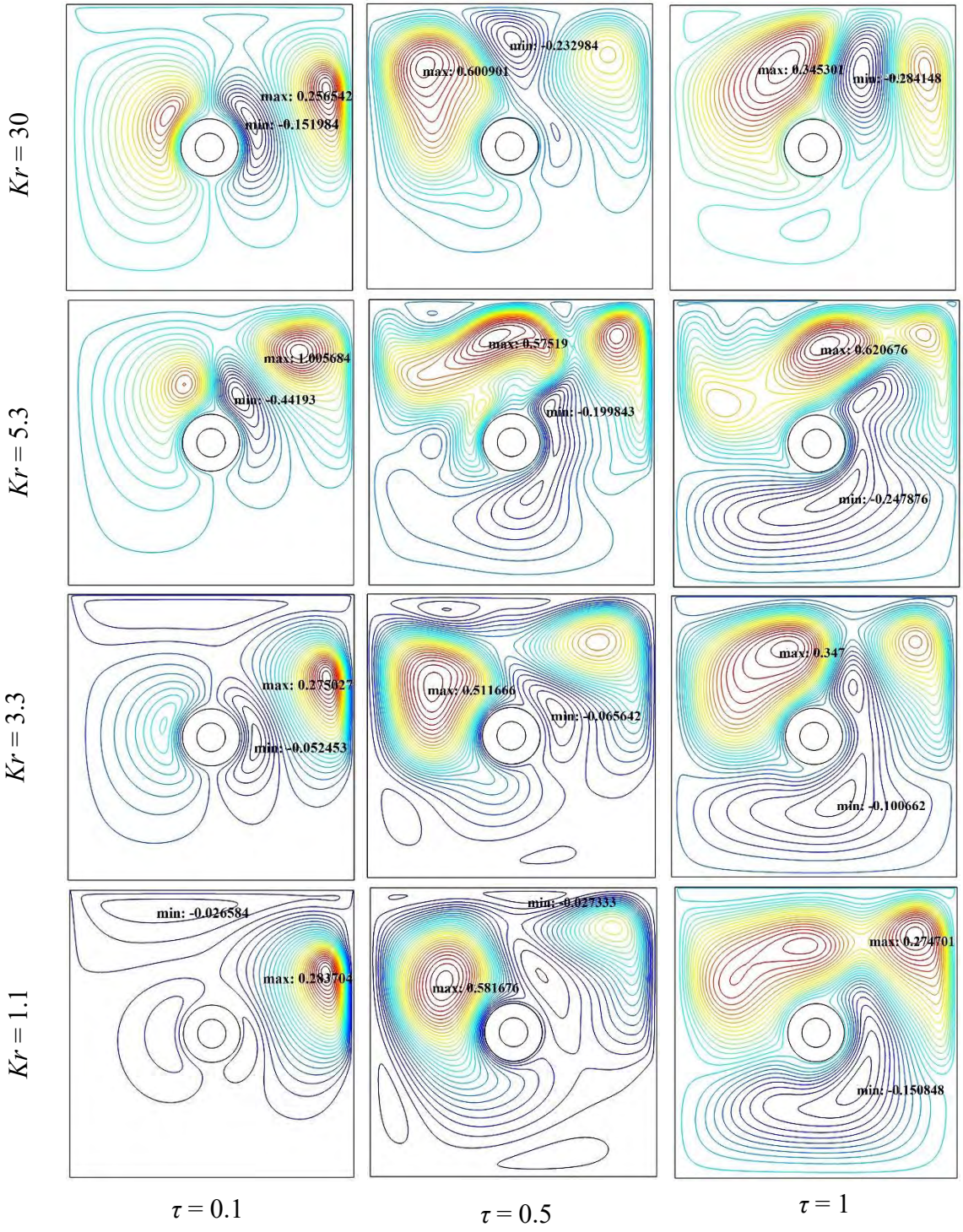


**Figure: 3.1.** Effect of thermal conductivity ratio (*Kr*) on streamlines for different dimensionless time ($\tau$) at $Re = 100$, $Pr = 0.71$, $Q = 0.2$, $Ri = 1$, $Lc = 0.3$.

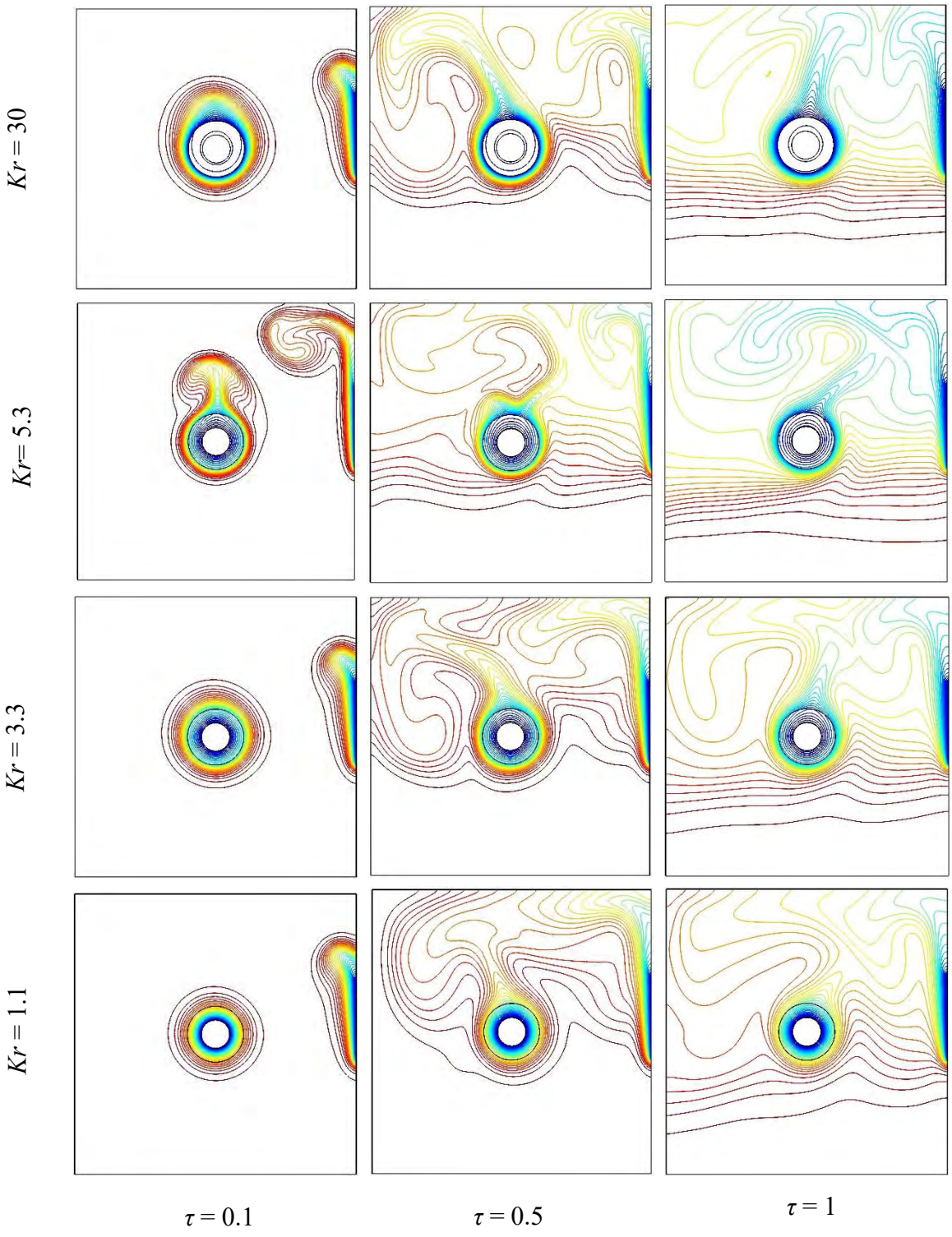


**Figure: 3.2.** Effect of thermal conductivity ratio (*Kr*) on isotherms for different dimensionless time ($\tau$) at $Re = 100$, $Pr = 0.71$, $Q = 0.2$, $Ri = 1$, $Lc = 0.3$.

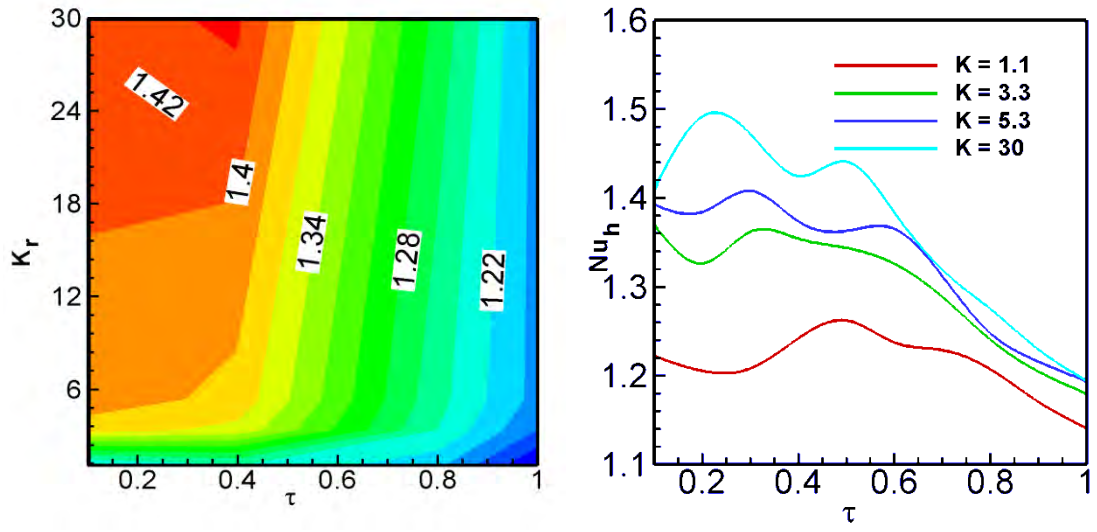


(a) (b)

**Figure: 3.3.** Effect of thermal conductivity ratio (*Kr*) and dimensionless time ($\tau$) on average heat transfer rate from the heated surface with (a) the contour plot and (b) the line graph at $Re = 100$, $Pr = 0.71$, $Q = 0.2$, $Ri = 1$, $Lc = 0.3$.

Isotherms are presented in Fig. 3.2 for same parameters as in Fig. 3.1. Temperature is distributed around the heat exchanger and plume like distribution is observed with increasing of thermal conductivity. Isotherms are distributed almost parallel to horizontal wall from top to bottom side of heat exchanger for $\tau = 1$. The corresponding isotherms results from the figure indicate that the lower valued isotherms are near the right side boundary and hollow cylinder cooler isothermal zone is found. So, right side wall and hollow cylinder contain lower temperature. At high thermal conductivity ratio the mixed convection plays a dominant role and the recirculation flow is mostly generated by the moving lid. From figure, 3.2 it is seen that the thermal conductivity ratio enhances from 1 to 30, the temperature contours tend to get effected considerably. At $Kr = 1.1$ and $\tau = 0.1$ the isothermal line near the hollow cylinder are spherical. But when $Kr = 30$ and $\tau = 0.1$ then the isothermal line near the hollow cylinder are elliptic. It is observed that the isothermal lines are denser near the hollow cylinder and right wall but isothermal lines are thinner near the upper lid since the upper lid is moving to the left and right with considerably higher velocity.

The effect of solid fluid thermal conductivity ratio ($Kr$) and dimensionless time ($\tau$) on average heat transfer rate from the heated surface with (a) the contour plot and (b) the line graph at $Re$ = 100, $Pr$ = 0.71, $Q$ = 0.2, $Ri$ = 1, $Lc$ = 0.3 are shown in figure 3.3 for different values of $Kr$. The figure 3.3(a), shows the distribution of the solid fluid thermal conductivity ratio ($Kr$) vs. the dimensionless time ($\tau$). In this case, if $Kr$ increases to 30 then the temperature decreases. From the figure 3.3(b), it is shown that the average Nusselt number remains unsteady and at last they are decreasing for different values of $Kr$. It is observed that the average Nusselt number for different $Kr$ shows an oscillatory phenomenon with increasing $\tau$. It is also noting that $Nu_h$ is always higher for bigger value of $Kr$.

### 3.2 EFFECT OF PRANDTL NUMBER

The effect of Prandtl number on the flow fields as streamlines in the cavity at three different values of $\tau$ is shown in the three different column of the figure 3.4, while $Re$ = 100, $Kr$ = 5.3, $Q$ = 0.2, $Ri$ = 1 and $Lc$ = 0.3. The flow fields are depicted for all values of $Pr$ (= 1, 2, 5, 10) here $Pr$ = 1 is for air, $Pr$ = 10 is for water and all values of $\tau$ (= 0.1, 0.5, 1). From figure 3.4, it is observed that when $\tau$ = 0.5 and $Pr$ = 1, 10 the maximum and minimum values of streamlines are same. Again when $\tau$ = 1 and $Pr$ = 1, 10 the maximum and minimum values are also same. Color indicates the strength of flow field, blue is for lower strength and red is for higher strength. Here, some maximum and minimum values for different values of Prandtl number are obtained. When $Pr$ = 1 and $\tau$ = 0.1, then the maximum value is near the right wall and minimum value is near the hollow cylinder. But when $Pr$ = 2, 5 and 10 then, the minimum values are near the upper wall which is moving with considerable higher velocity. Almost all the vortex points which carries different maximum and minimum values are elliptic. For $\tau$ = 0.5 and 1 multiple cells are formed. While $\tau$ changes from 0.1 to 0.5 extra eddy is appeared at the right corner of the cavity. The size of the eddy increases with the higher values of $Pr$. This indicates that the fluid flow of the enclosure has been affected by the inertia force.

The effect of Prandtl number for thermal field in the cavity at three different values of $\tau$, while $Re$ = 100, $Kr$ = 5.3, $Q$ = 0.2, $Ri$ = 1 and $Lc$ = 0.3 is shown in figure 3.5.

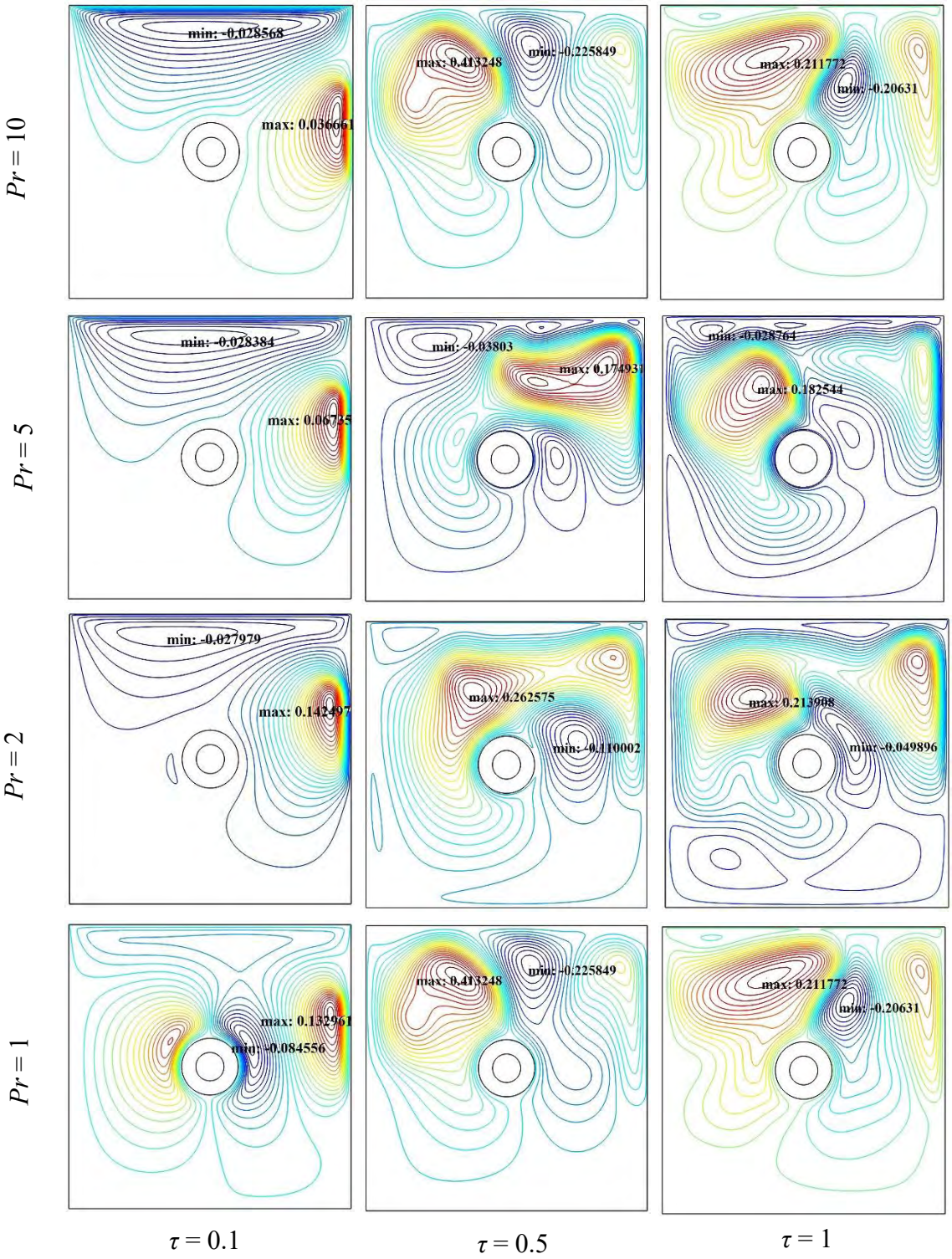


**Figure: 3.4.** Effect of Prandtl number (*Pr*) on streamlines for different dimensionless time ($\tau$) at $Re = 100$, $Kr = 5.3$, $Q = 0.2$, $Ri = 1$, $Lc = 0.3$.

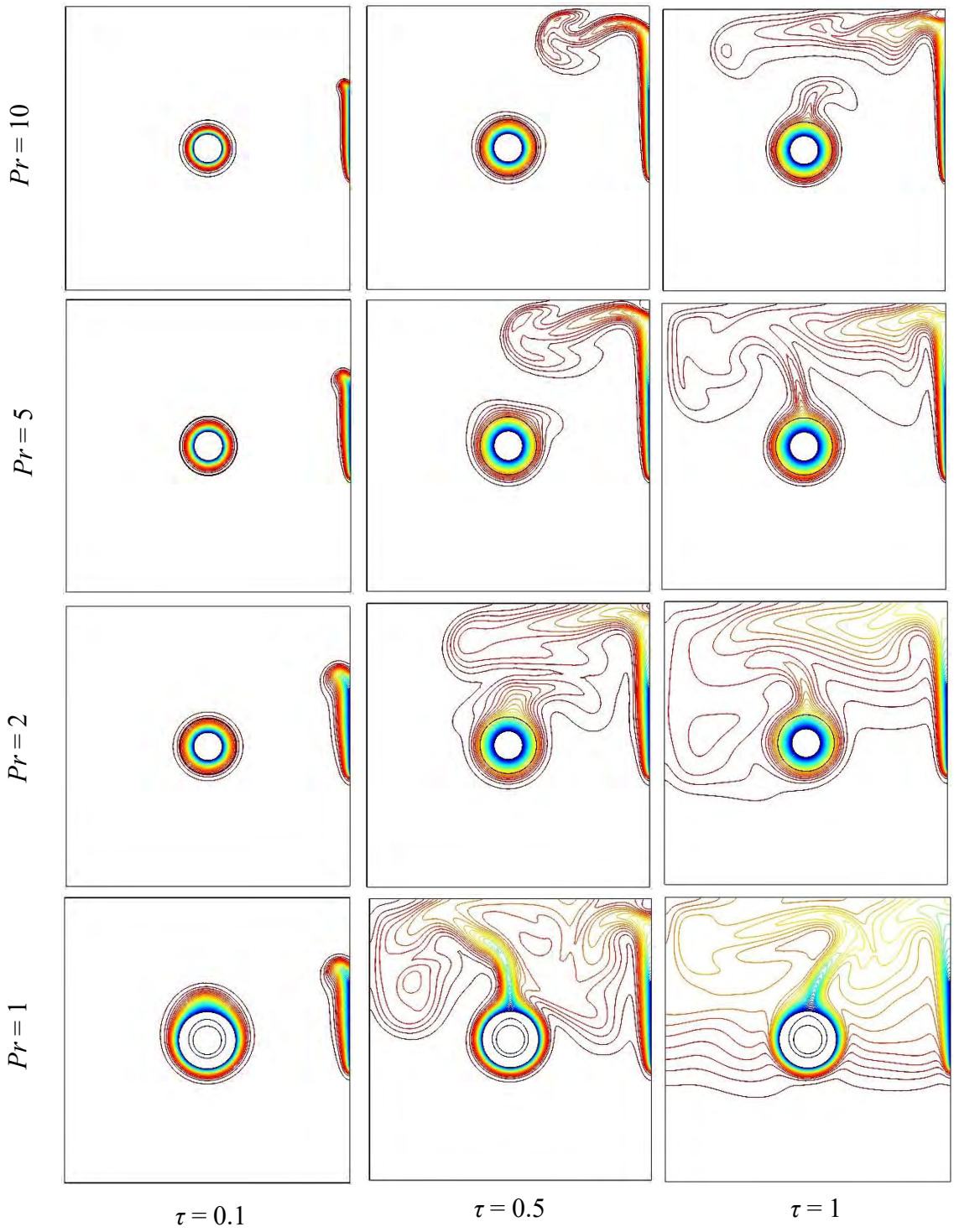


**Figure: 3.5.** Effect of Prandtl number (*Pr*) on isotherms for different dimensionless time ($\tau$) at $Re = 100$, $Kr = 5.3$, $Q = 0.2$, $Ri = 1$, $Lc = 0.3$.

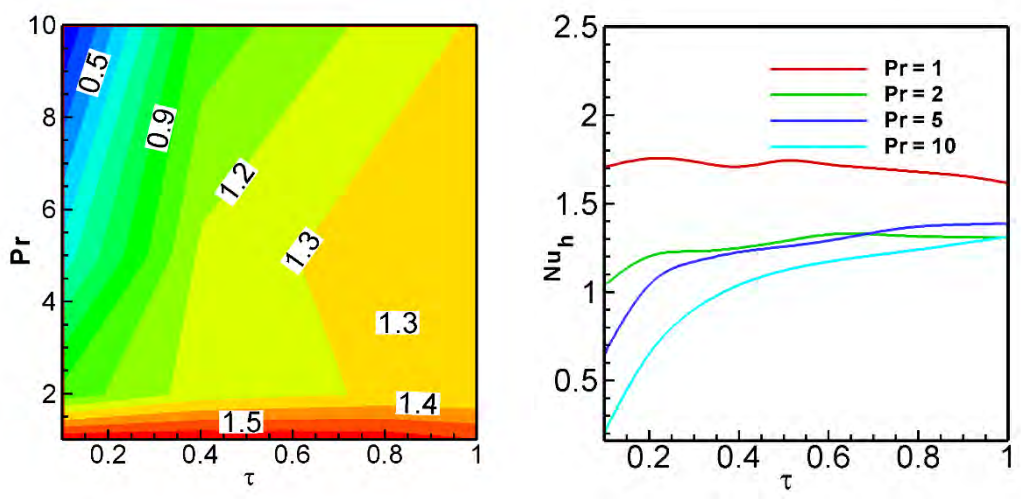


(a) (b)

**Figure: 3.6.** Effect of Prandtl number (*Pr*) and dimensionless time ($\tau$) on average heat transfer rate from the heated surface with (a) the contour plot and (b) the line graph at $Re = 100$, $Kr = 5.3$, $Q = 0.2$, $Ri = 1$, $Lc = 0.3$.

By the increasing values of *Pr* the plume like isothermal lines are decreasing when $\tau = 0.1$. Thermal boundary layer thickness increases and the isothermal lines become thinner and closer at the adjacent area of the heat source as $\tau$ increases in the convection regimes. There are also noticeable changes in temperature field with various $\tau$ is shown for a fixed *Pr*. This is because of the significant influence of increasing $\tau$ on isotherms. At low values of *Pr* the spread of isotherms is due to a strong stream wise conduction that decreases the stream wise temperature gradient in the field.

The effect of Prandtl number (*Pr*) and dimensionless time ($\tau$) on average heat transfer rate from the heated surface with (a) the contour plot and (b) the line graph at $Re = 100$, $Kr = 5.3$, $Q = 0.2$, $Ri = 1$ and $Lc = 0.3$ is shown in figure 3.6. In contour plot figure 3.6(a), it is shown that with the higher values of *Pr* and lower value of $\tau$ average heat transfer rate is lowest and for almost all values of $\tau$ with low *Pr* heat transfer rate is high. From figure 3.6(b), it is clearly observed that the variation of the average Nusselt number ($Nu_h$) at the heat generating source is increasing with the increasing value of *Pr* except $Pr = 1$. The average Nusselt number goes up quickly with increasing *Pr* for the aforesaid values of $\tau$.

### 3.3 EFFECT OF HEAT GENERATION PARAMETER

The effect of heat generation parameter on the flow fields as streamlines in the cavity at three different values of dimensionless time ($\tau$) is presented in the three different columns of the figure 3.7, while $Re$ = 100, $Kr$ = 5.3, $Pr$ = 0.71, $Ri$ = 1 and $Lc$ = 0.3. Here, the color indicates the temperature of flow field, red is for higher temperature and blue color indicates lower temperature. Here, some maximum and minimum values are obtained for different values of heat generation parameter ratio. From figure 3.7, it is clearly observed that the flow field remains almost same at different values of $\tau$ for all values of $Q$. When, $\tau$ = 0.1 the maximum and minimum values and position are almost same for all values of $Q$. There is no significant change in flow patterns for all the values of heat generation parameter ($Q$) at the dominant mixed convection region.

The effect of heat generation parameter ($Q$) on isotherms for different dimensionless time ($\tau$) at $Re$ = 100, $Kr$ = 5.3, $Pr$ = 0.71, $Ri$ = 1 and $Lc$ = 0.3 is shown in figure 3.8. The figure provides the information about the influence of $Q$ at the three different values of $\tau$ on isotherms. It is clearly observed that the isothermal lines are same for the increasing values of $Q$ with three different dimensionless time ($\tau$).

The effect of heat generation parameter ($Q$) and dimensionless time ($\tau$) on average heat transfer rate from the heated surface with (a) the contour plot and (b) the line graph at $Re$ = 100, $Kr$ = 5.3, $Pr$ = 0.71, $Ri$ = 1 and $Lc$ = 0.3 are shown in figure 3.9. In contour plot figure 3.9(a), it is shown that the value is decreasing with the increasing value of $\tau$. From figure 3.9 (b), it is clearly observed that the variation of the average Nusselt number ($Nu_h$) at the heat generating source is decreasing generally with increasing value of $\tau$ due to the increasing effect of convection. These values of $Nu_h$ is the highest for lower value of $Q$ for every possible time steps τ.

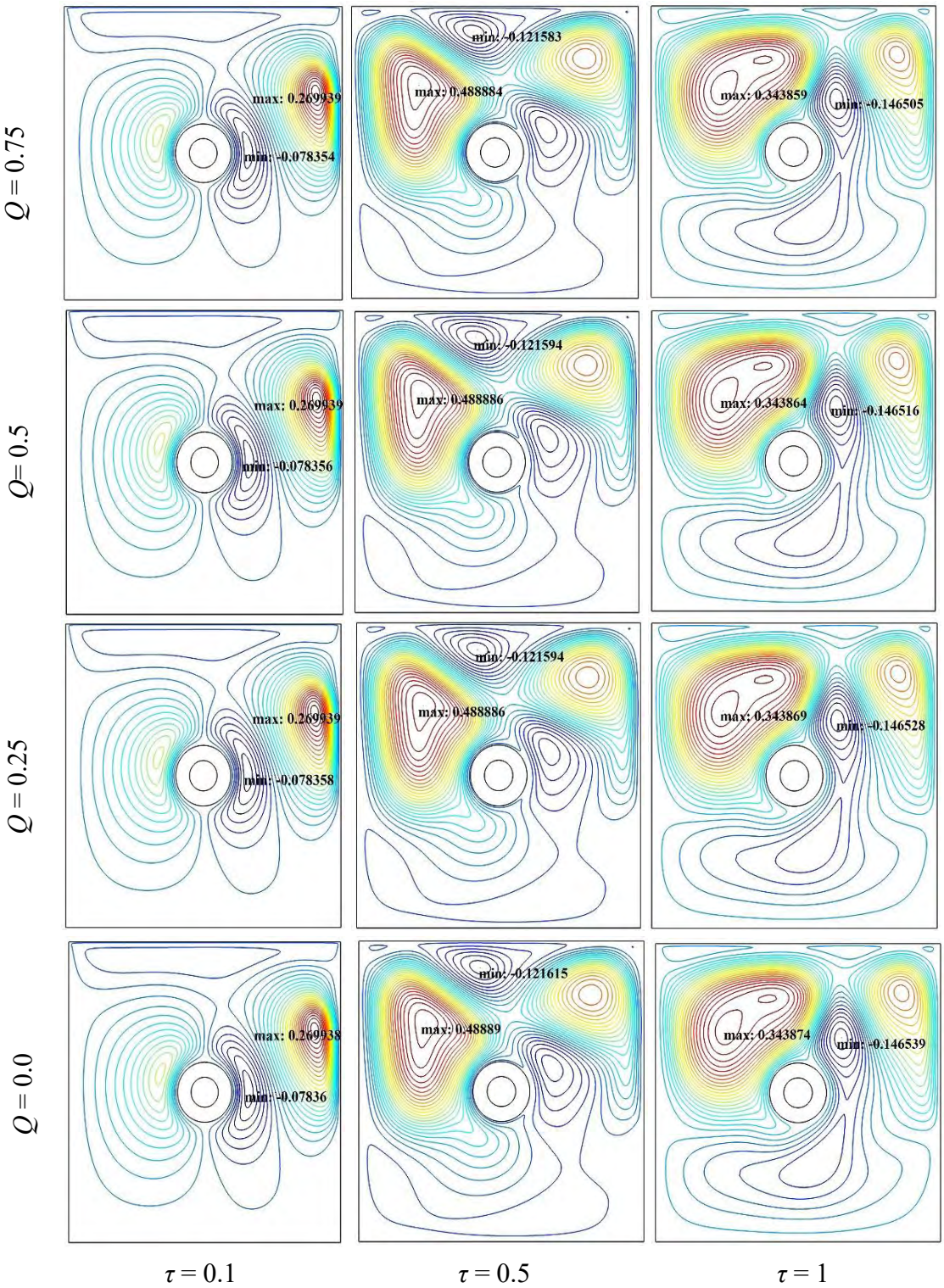


**Figure: 3.7.** Effect of heat generation parameter ($Q$) on streamlines for different dimensionless time ($\tau$) at $Re$ = 100, $Kr$ = 5.3, $Pr$ = 0.71, $Ri$ = 1, $Lc$ = 0.3.

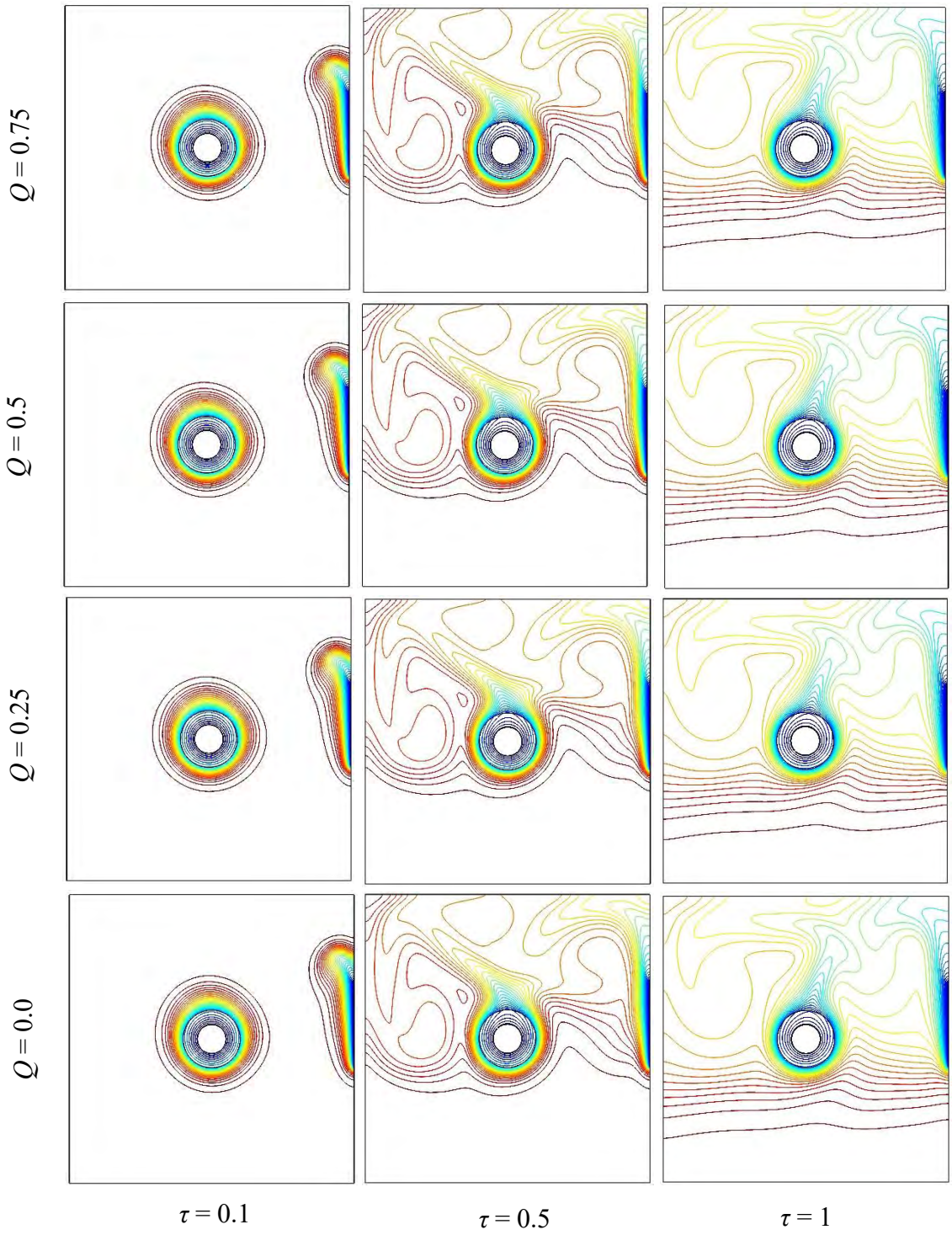


**Figure: 3.8.** Effect of heat generation parameter ($Q$) on isotherms for different dimensionless time ($\tau$) at $Re$ = 100, $Kr$ = 5.3, $Pr$ = 0.71, $Ri$ = 1, $Lc$ = 0.3.

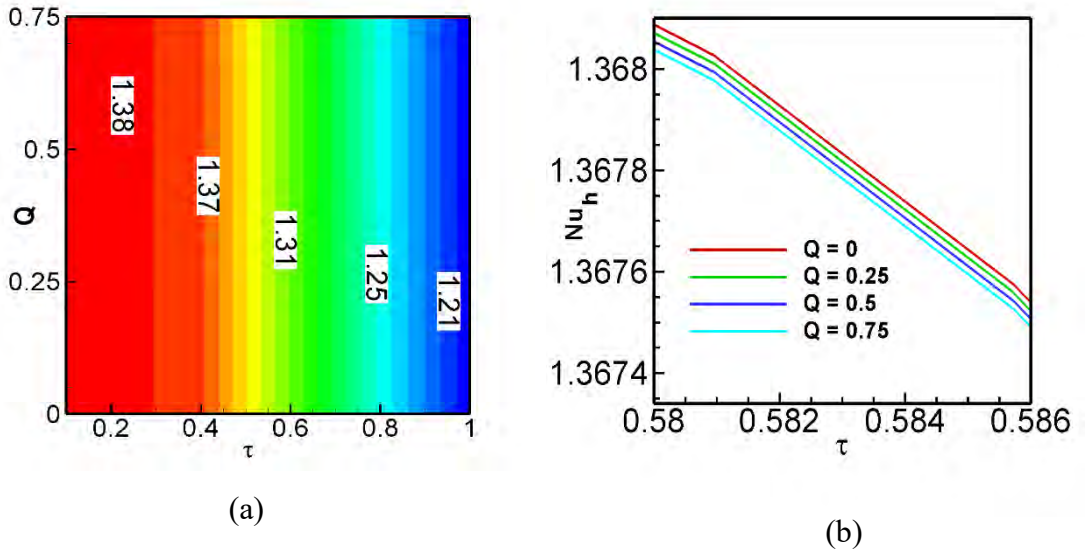


(a) (b)

**Figure: 3.9.** Effect of heat generation parameter ($Q$) and dimensionless time ($\tau$) on average heat transfer rate from the heated surface with (a) the contour plot and (b) the line graph at $Re$ = 100, $Kr$ = 5.3, $Pr$ = 0.71, $Ri$ = 1, $Lc$ = 0.3.

### 3.4 EFFECT OF COOLING LENGTH

The effect of cooling length ($Lc$) on flow field as streamline in the cavity while $Re$ = 100, $Pr$ = 0.71, $Q$ = 0.2, $Ri$ = 1, $Kr$ = 5.3 at times dimensionless time $\tau$ (0.1, 0.5, 1) are displayed in the column of the figure 3.10. For all values of $Lc$, number of cells is equal for all values of $\tau$. A kidney shaped cell is formed for $\tau$ = 0.1 at right side of heat exchanger and it carries minimum values. Another cell is sited at the right side near the right wall and it carries maximum values. Both cells are changing their position for $\tau$ = 0.5 and 1. Multiple cells are formed for the highest values of $\tau$ which indicates the increase of convection.

The effect of cooling length ($Lc$) on isotherms for different dimensionless time ($\tau$) at $Re$ = 100, $Pr$ = 0.71, $Q$ = 0.2, $Ri$ = 1, $Kr$ = 5.3 are shown in figure 3.11. Plume like distribution is observed with the increasing values of $\tau$. Temperature is distributed around the heat exchanger. Isotherms are distributed almost parallel to horizontal wall from top to bottom side of heat exchanger. When $\tau$ = 0.1, the isothermal lines near the right wall are increasing with the increasing values of cooling length.

The effect of cooling length ($Lc$) and dimensionless time ($\tau$) on average heat transfer rate from the heated surface with (a) the contour plot and (b) the line graph at $Re$ = 100, $Pr$ = 0.71, $Q$ = 0.2, $Ri$ = 1, $Kr$ = 5.3 are shown in figure 3.12. From figure 3.12(a),

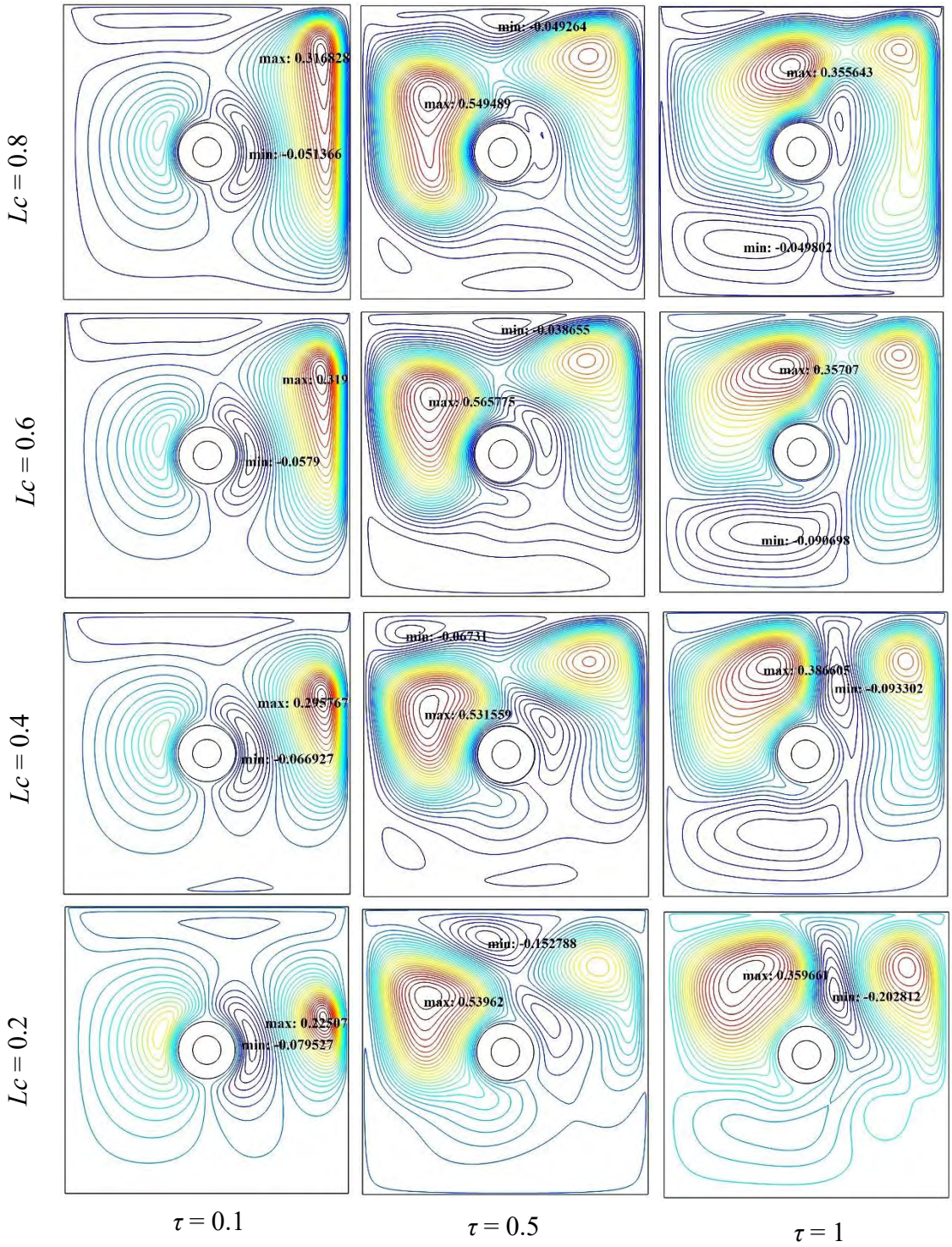


**Figure: 3.10.** Effect of cooling length (*Lc*) on streamlines for different dimensionless time ($\tau$) at $Re = 100$, $Kr = 5.3$, $Q = 0.2$, $Ri = 1$, $Pr = 0.71$.

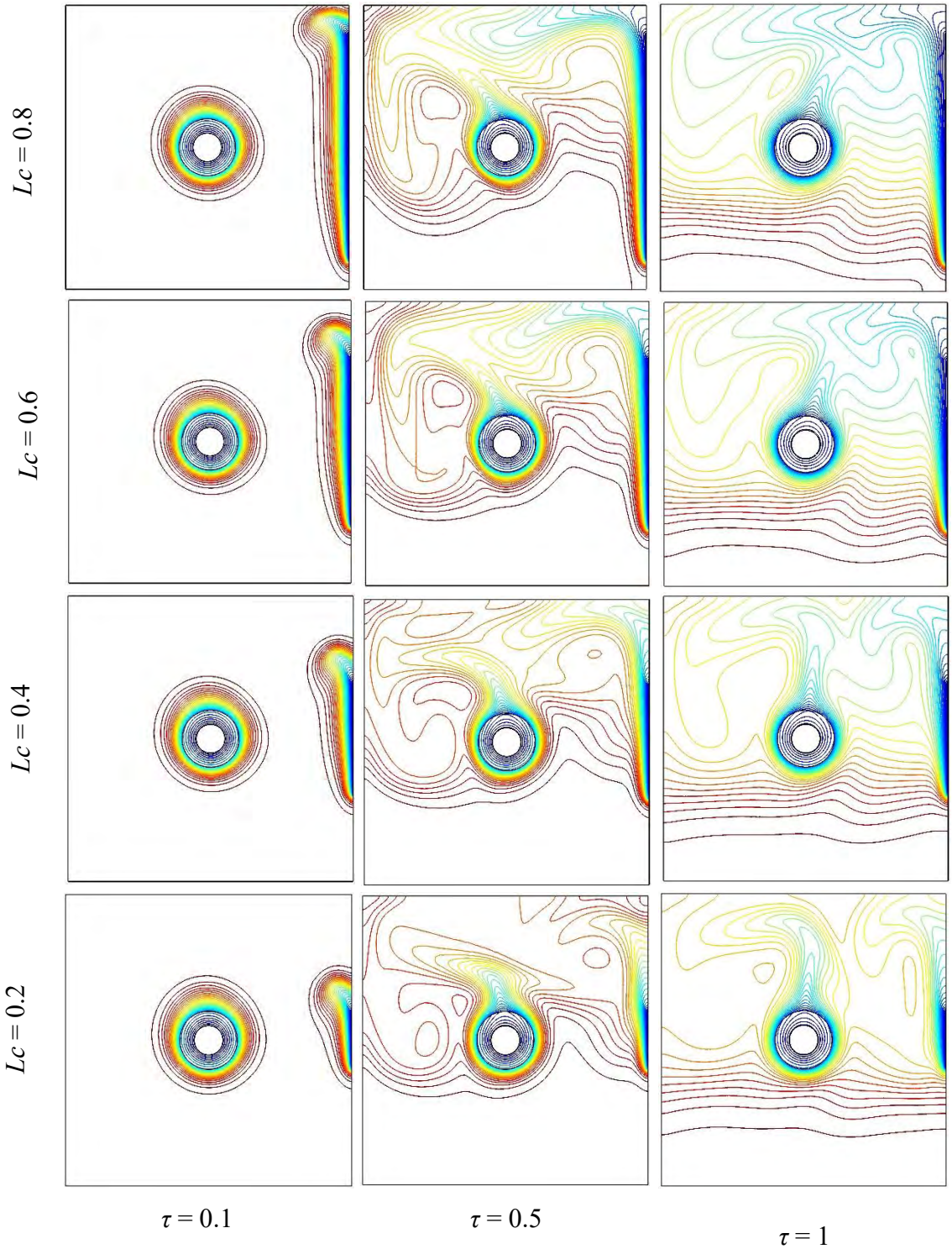


**Figure: 3.11.** Effect of cooling length ($Lc$) on isotherms for different dimensionless time ($\tau$) at $Re = 100$, $Kr = 5.3$, $Q = 0.2$, $Ri = 1$, $Pr = 0.71$.

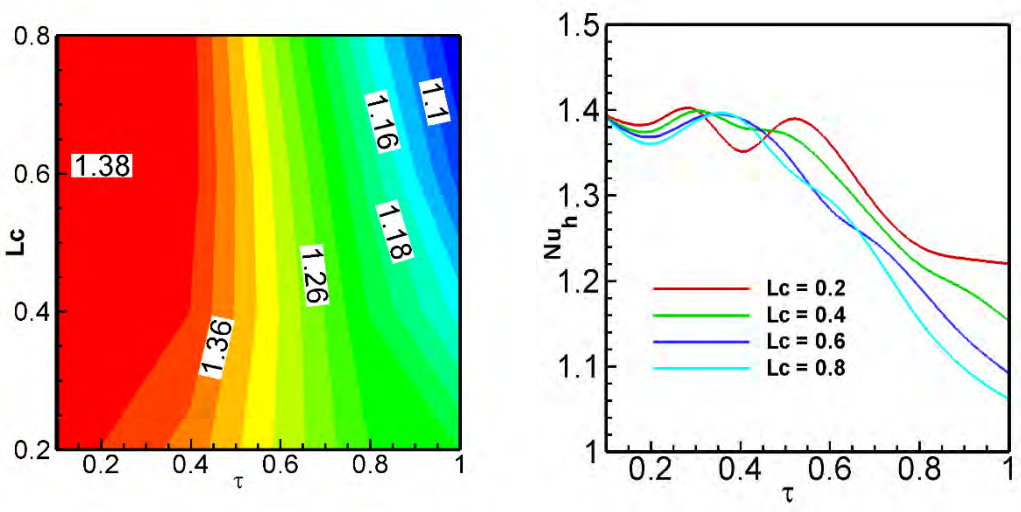


(a) (b)

**Figure: 3.12.** Effect of cooling length (*Lc*) and dimensionless time ($\tau$) on average heat transfer rate from the heated surface with (a) the contour plot and (b) the line graph at $Re = 100$, $Kr = 5.3$, $Q = 0.2$, $Ri = 1$, $Pr = 0.71$.

it is seen that the average heat transfer rate are initially high for all length of the cooler and then decreases gradually with increasing values of $\tau$. From figure 3.12(b), it is seen that the temperature in the cavity increases up to a certain value of $\tau$ then it decreases for increasing value of $\tau$. For all values of *Lc*, $Nu_h$ shows an oscillatory behavior.

### 3.5 EFFECT OF RICHARDSON NUMBER

The effect of Richardson number on the flow fields as streamlines in the cavity at three different values of dimensionless time ($\tau$) is shown in the three different column of the figure 3.13, while $Re = 100$, $Kr = 5.3$, $Q = 0.2$, $Lc = 0.3$, $Pr = 0.71$. Here the left and right walls are adiabatic and the upper wall is moving right side. The movement of the lid causes two primary vortices to be formed, one is near the lid and another is near the right wall or left wall or near the heat generating obstacle. These vortices carry maximum and minimum values. Multiple cells are formed for the increasing values of $\tau$. All the vortices are elliptic in size. The previously existing vortices are nearer to the side walls and new vortices are formed near the other walls and heat generating object which illustrates the increment in the velocity of the fluid.

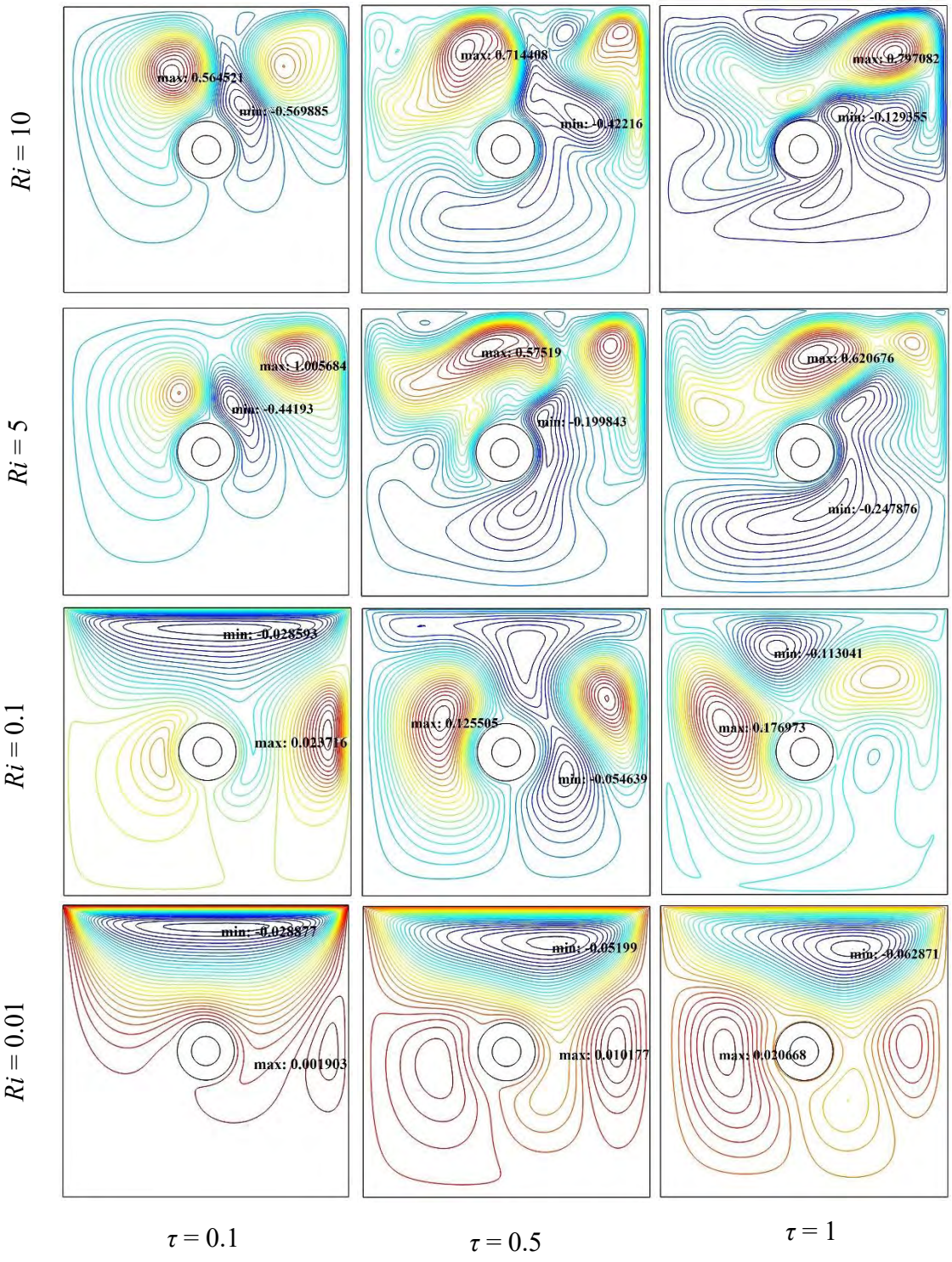


**Figure: 3.13.** Effect of Richardson number (*Ri*) on streamlines for different dimensionless time ($\tau$) at $Re = 100$, $Kr = 5.3$, $Q = 0.2$, $Lc = 0.3$, $Pr = 0.71$.

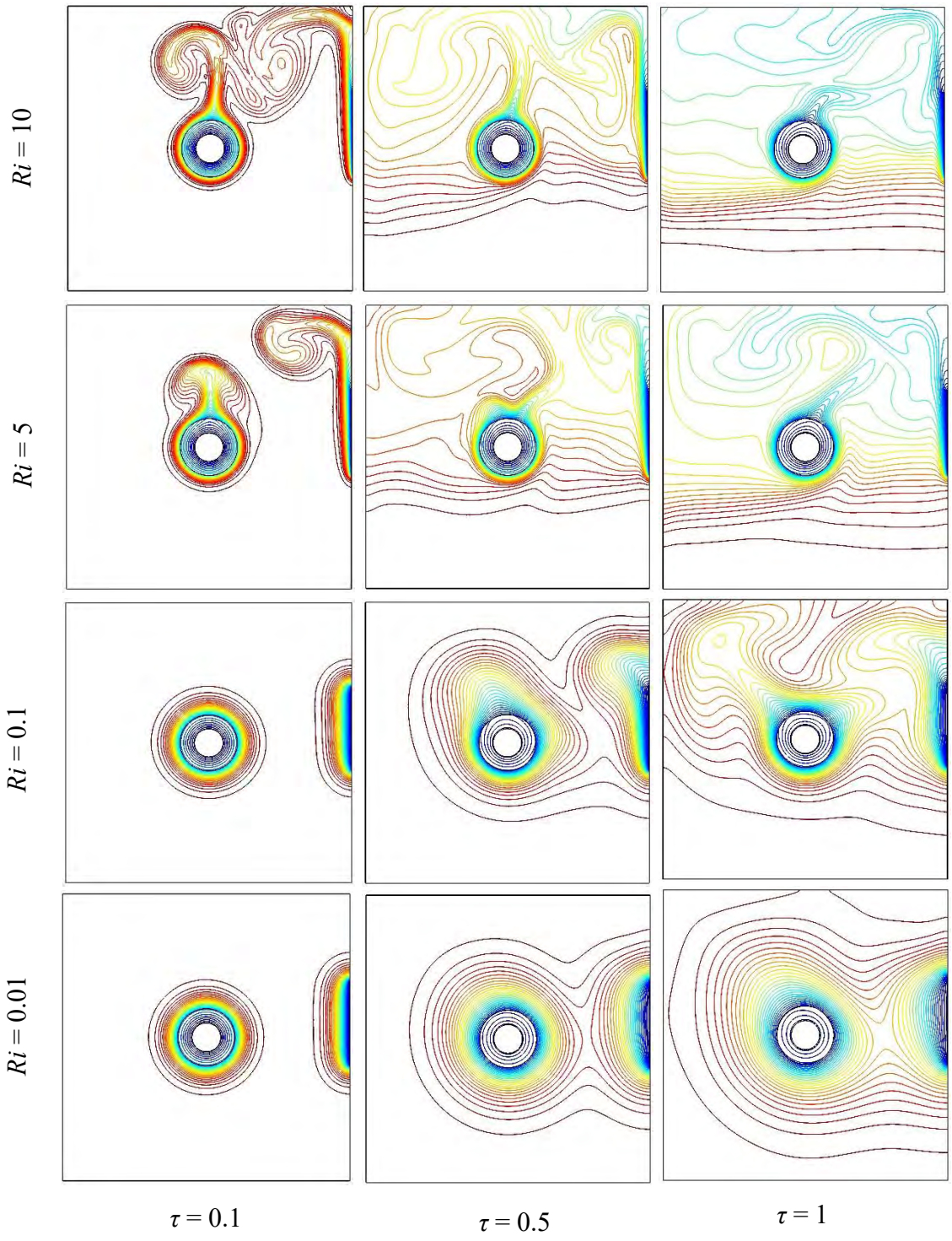


**Figure: 3.14.** Effect of Richardson number (*Ri*) on isotherms for different dimensionless time ($\tau$) at $Re = 100$, $Kr = 5.3$, $Q = 0.2$, $Lc = 0.3$, $Pr = 0.71$.

The effect of Richardson number for thermal field in the cavity at three different values of $\tau$, while $Re$ = 100, $Kr$ = 5.3, $Q$ = 0.2, $Pr$ = 0.71 and $Lc$ = 0.3 are shown in figure 3.14. The figure shows the information about the influence of Richardson number at the different values of $\tau$ on isotherms. When $Ri$ = 0.01 and 0.1 the isotherms demonstrate that temperature gradient near the right wall and at $Ri$ = 5 and 10 the isothermal lines are increasing and join with the heat generating isothermal lines. For different dimensionless time ($\tau$) the isothermal lines are almost parallel and it is distributed to the horizontal top wall to bottom side of the generating solid object. The isotherms near the right wall in the cooling part are looked like the shadow.

The effect of Richardson number ($Ri$) and dimensionless time ($\tau$) on average heat transfer rate from the heated surface with (a) the contour plot and (b) the line graph at $Re$ = 100, $Kr$ = 5.3, $Q$ = 0.2, $Pr$ = 0.71 and $Lc$ = 0.3 is shown in figure 3.15.

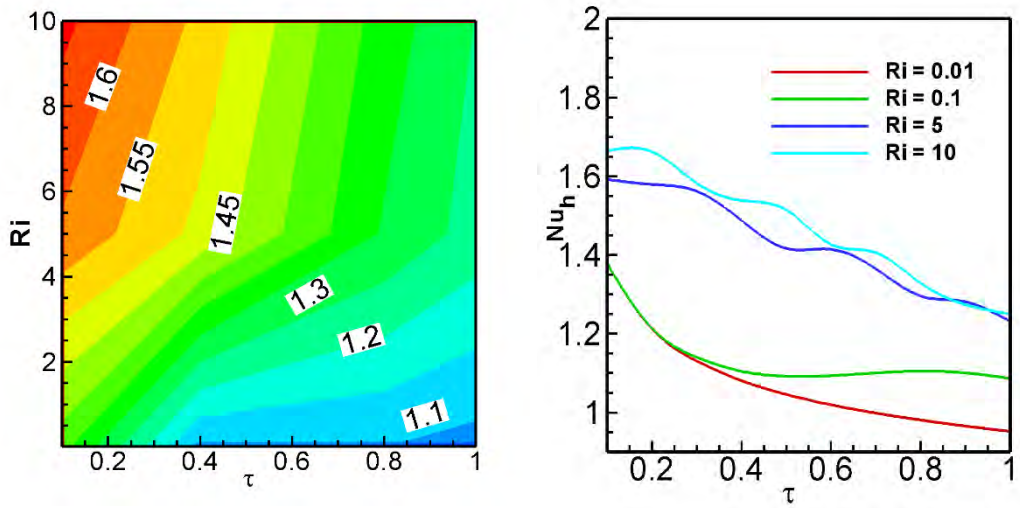


(a) (b)

**Figure: 3.15.** Effect of Richardson number ($Ri$) and dimensionless time ($\tau$) on average heat transfer rate from the heated surface with the (a) contour plot and (b) line graph at $Re$ = 100, $K$ = 5.3, $Q$ = 0.2, $Lc$ = 0.3, $Pr$ = 0.71.

The first figure 3.15(a), is for contour plot of heat transfer rate for Richardson number ($Ri$) vs dimensionless time ($\tau$) which shows that when the values of $\tau$ increases and the Richardson number decreases, heat transfer rate decreases and vice versa. Again from figure 3.15(b), when $Ri$ = 0.01 the average Nusselt number decreases more rapidly with time comparative to when $Ri$ = 0.1. At $Ri$ = 5 and 10 the temperature are decreasing for the increasing values of $\tau$. It is higher for the large value of $Ri$ and lower for the small value of $Ri$.

### 3.6 EFFECT OF REYNOLDS NUMBER

The effect of Reynolds number on the flow structure and temperature distribution is depicted in figure 3.16. The streamlines are presented for different values of Reynolds numbers ranging from 50 to 500 respectively while $Ri$ = 1, $Kr$ = 5.3, $Q$ = 0.2, $Lc$ = 0.3, $Pr$ = 0.71. From figure 3.16, it is observed that when, $\tau$ = 0.01 and $Re$ = 50 the streamlines are thick but with the increasing values of $Re$ the streamlines are become thinner. Here, we get some maximum and minimum values. Maximum values are near the right wall and here the streamlines are thick, minimum values are near the heat generating object and here the streamlines are thin. When the values of $\tau$ are increasing the vortex which carries maximum and minimum values change their position and another small vortex is induced. The size of the vortex as well as the flow strength has a strong effect as the $Re$ is increased. The flow field is almost symmetrical adjacent of the side walls for all values of $Re$.

The corresponding isotherm pattern for Reynolds number for thermal field in the cavity at different values of $\tau$ while $Ri$ = 1, $Kr$ = 5.3, $Q$ = 0.2, $Lc$ = 0.3, $Pr$ = 0.71 is shown in figure 3.17. In this figure, it is found that the isotherm are more tightened at the vicinity of the heated wall of the cavity which shows the noticeable increase in convection heat transfer. The cavity is heated from the middle side and has a higher concentration compared to the other boundaries of the cavity. Plume-like distribution is observed starting from the right side of the cavity. An interesting result can be explained through the flow of movement inside the cavity which goes on to develop for $\tau$ = 0.5 and $\tau$ = 1. At $\tau$ = 1 and $Re$ = 50 the isotherms are almost parallel near the bottom wall but for the increasing value of $Re$ the isotherms are become condensed in the vicinity of the heated obstacle.

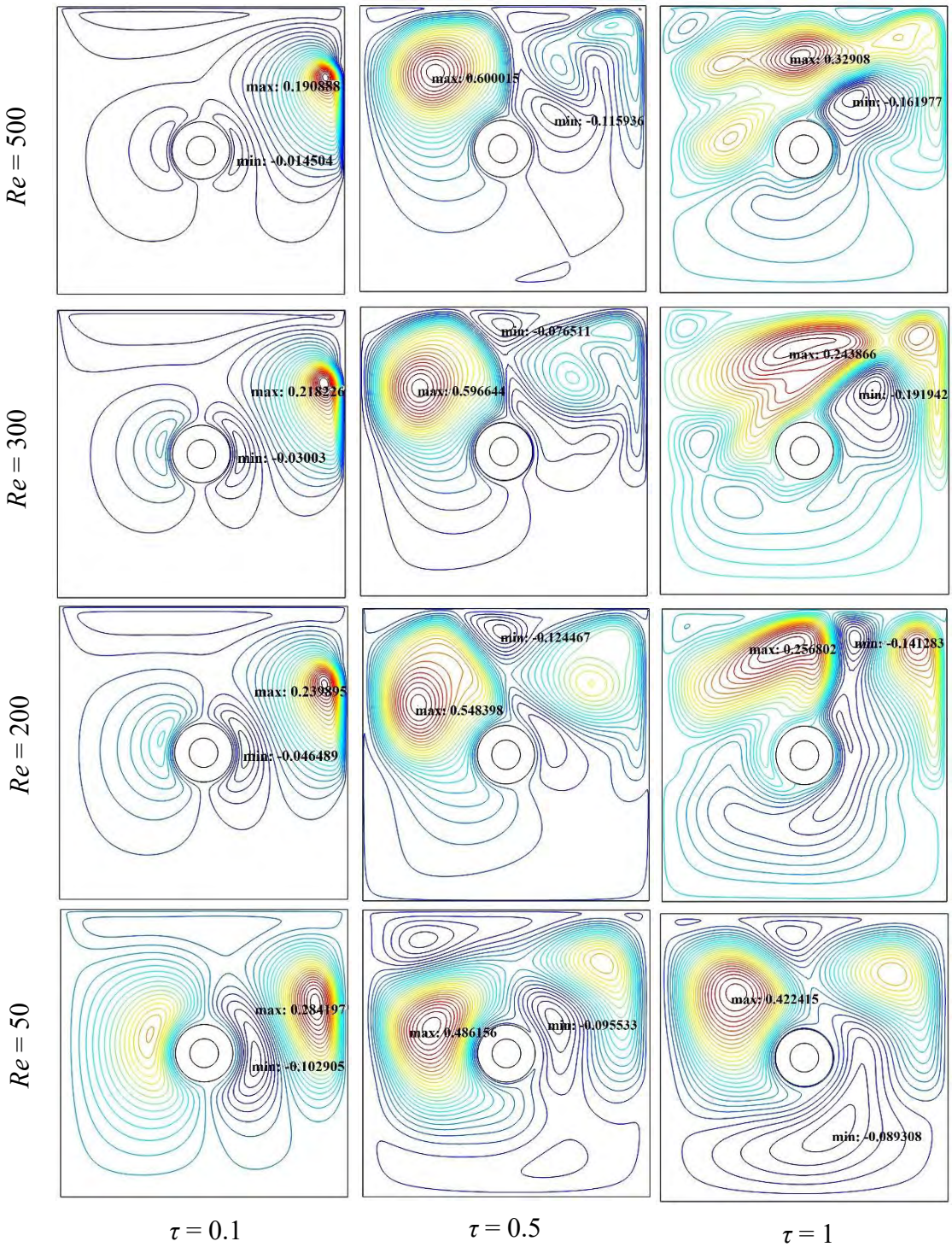


**Figure: 3.16.** Effect of Reynolds number (*Re*) on streamline for different dimensionless time ($\tau$) at $Ri = 1$, $Kr = 5.3$, $Q = 0.2$, $Lc = 0.3$, $Pr = 0.71$.

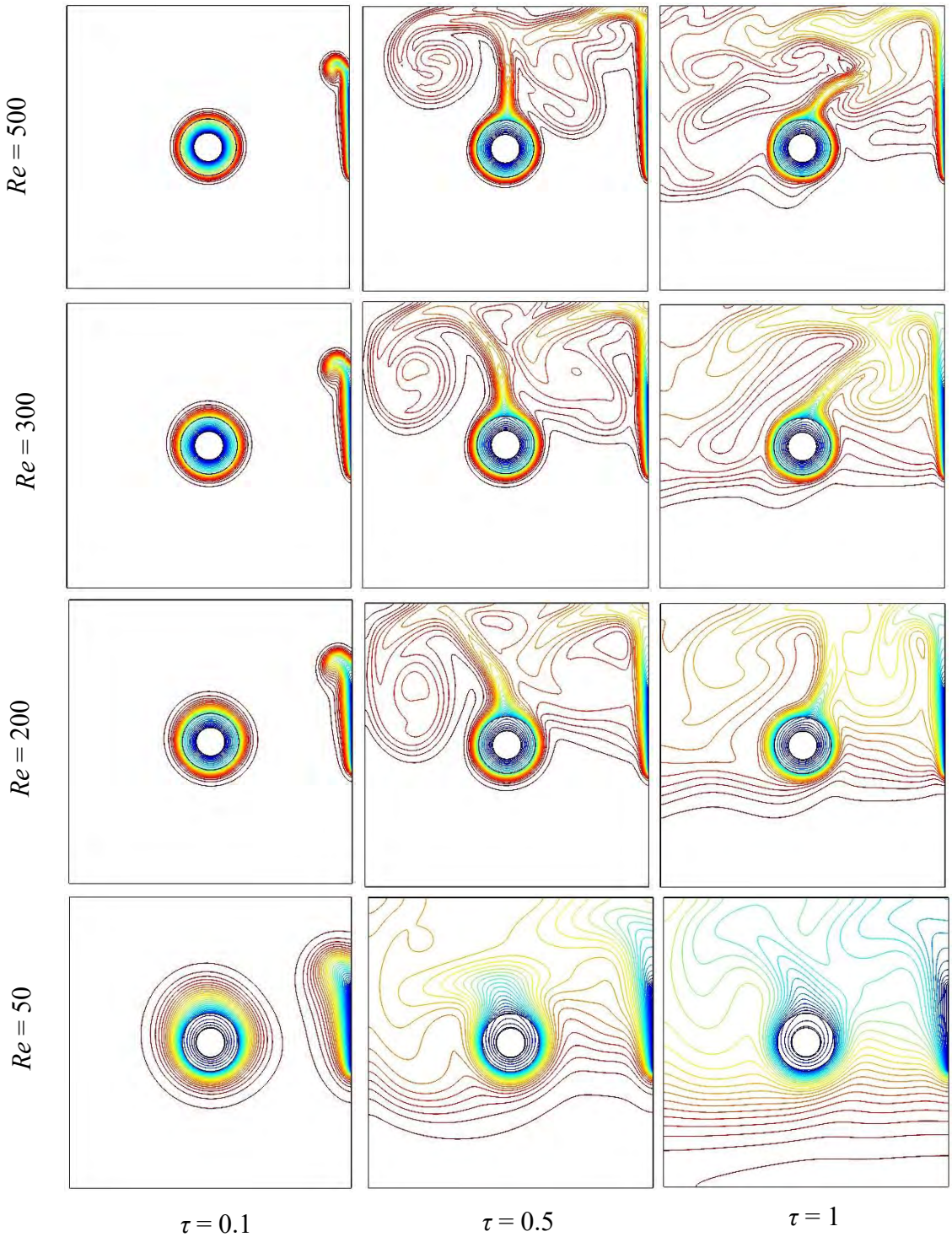


**Figure: 3.17.** Effect of Reynolds number (*Re*) on isotherms for different dimensionless time ($\tau$) at $Ri = 1$, $Kr = 5.3$, $Q = 0.2$, $Lc = 0.3$, $Pr = 0.71$.

The effect of Reynolds number ($Re$) and dimensionless time ($\tau$) on average heat transfer rate from the heated surface with (a) the contour plot and (b) the line graph at $Ri$ = 1, $Kr$ = 5.3, $Q$ = 0.2, $Lc$ = 0.3, $Pr$ = 0.71 is shown in figure 3.18. From figure 3.18(a), it is found that $Re$ =0-300 with the increase of $\tau$ and decrease of $Re$, heat transfer rate declines. For $Re$ > 300 with the increase of $\tau$ a different pattern is observed for heat transfer. From figure 3.18(b), it is observed that the average Nusselt number at the heated surface is primarily high for all values of Re, and as $\tau$ increases after a certain level average Nusselt number decreases slowly for the rest values of $\tau$. It is also note that $Nu_h$ is higher for $Re$ = 500 and the lower value of $Nu_h$ is observed for $Re$ = 50.

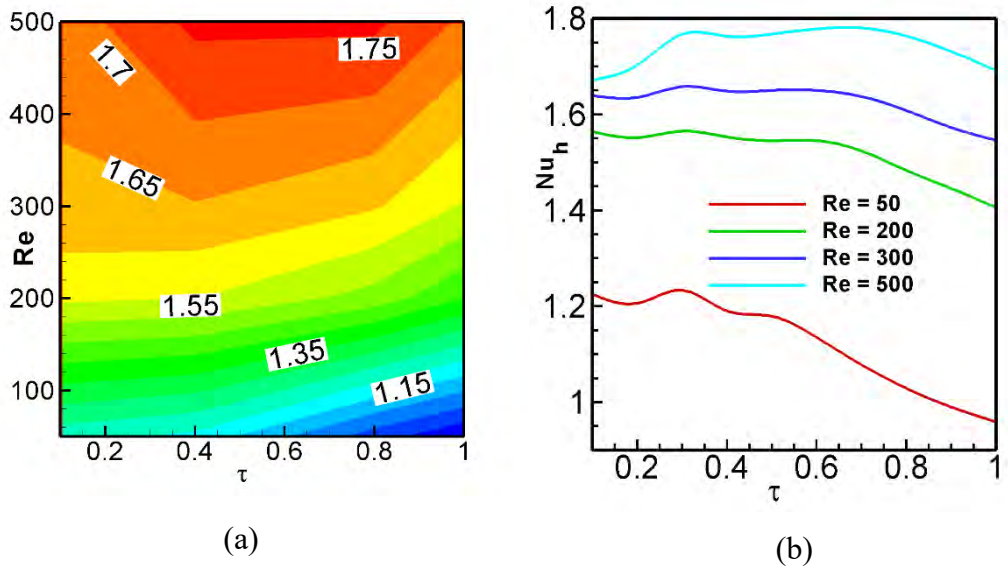


**Figure: 3.18.** Effect of Reynolds number ($Re$) and dimensionless time ($\tau$) on average heat transfer rate from the heated surface with the (a) contour plot and (b) line graph at $Ri$ = 1, $Kr$ = 5.3, $Q$ = 0.2, $Lc$ = 0.3, $Pr$ = 0.71.

# CHAPTER 4

# CONCLUSIONS

Mixed convection heat transfer from double-pipe heat exchanger in a partially cooled enclosure has been investigated numerically. The results are presented for thermal fields and flows inside the cavity. The sidewalls are kept adiabatic and the upper wall is moving both the direction. The heat generating object hollow cylinder is placed at the center of the cavity. Finite element method is used to solve governing equations and appropriate boundary conditions. The effect of different dimensionless parameters like thermal conductivity ratio (*Kr*), Prandtl number (*Pr*), heat generation parameter (*Q*), cooling length (*Lc*), Richardson number (*Ri*), and Reynolds number (*Re*) have been reported. Comparisons with the beforehand are performed and found to be in excellent agreement. The various ideas and results have been discussed in individual detail at the relevant chapter of the thesis. In the present chapter, an attempt is made to summaries the concepts and results obtained in the work reported already. A section on the scope of further work on associated fields of investigation is also included.

## 4.1 SUMMARY OF THE MAJOR OUTCOMES

The analysis has been confined to case of lid driven cavity containing hollow cylinder. On the basis of the analysis, the following conclusions could be drawn:

(i) The solid fluid thermal conductivity ratio (*Kr*) has a strong influence on thermal fields. There is a significant effect on streamlines for the increasing values of *Kr*. The thermal conductivity ratio (*Kr*) strongly effects the isotherms in the entire cavity. The average Nusselt number ($Nu_h$) remains unsteady and it decreases for different values of *Kr* and shows an oscillatory patterns with increasing dimensionless time ($\tau$).

(ii) Smaller Prandtl number (*Pr*) are more sensitive to the change of the buoyancy force than fluids having higher Prandtl number. In streamline, the size of the eddy increases with the improving values of *Pr*. Thermal boundary layer thickness increases and the isothermal lines become thinner and closer. The average Nusselt number ($Nu_h$) goes up quickly with increasing values of Prandtl number (*Pr*) for the aforesaid values of dimensionless time ($\tau$).

(iii) At the dominant mixed convection region there is no significant change in flow patterns for various values of heat generation parameter ($Q$). The isothermal lines remained same with the increase of $Q$. The average Nusselt number ($Nu_h$) at the heat generating source decreases with increase value of dimensionless time ($\tau$).

(iv) There is a notable effect of cooling length ($Lc$) on streamlines, isotherms and heat transfer rate. In streamlines, for the highest values of $\tau$ it shows multiple cells. Isotherms are distributed almost parallel to horizontal wall and heat is captured inside the cavity. The temperature increases up to a certain value of $\tau$ then it decreases for increase of $Lc$.

(v) There is a significant effect on streamlines, isothermal lines and heat transfer rate and these are presented for different values of $Ri$. Multiple elliptic cells are formed for the increase of $\tau$ and those are elliptic in size. The isothermal lines to be almost parallel by the increasing values of $\tau$. The average Nusselt number ($Nu_h$), $Ri$ decreases for the increase of dimensionless time ($\tau$).

(vi) When the values of $\tau$ are increasing the vortex change their position for different Reynolds number. The flow field was almost symmetrical adjacent to the side walls cavity which was heated from the middle side having a higher concentration compared to the other boundaries of the cavity. The average temperature increase up to a certain level and then decrease slowly for the rest of the values of $\tau$.

## 4.2 FURTHER WORKS

The following can be put forward for the further works as follow-ups of the present research:

- The study can be extended by internal heat generation, incorporating radiation effects and capillary effects in future.
- The porous medium can be investigated by changing the boundary position of the cavity wall and using magnetic fluids instead of electrically conducting fluids.
- Double expansion mixed convection can be analyzed with management equations of concentration preservation.

- In this thesis, heat transfer and two-dimensional fluid flow has been analyzed. This discussion can be extended to three-dimensional analysis to investigate the effect of parameter on flow fields and heat transfer in cavities.
- Single phase flow model is considered. Two phase models may be analyzed and compared to the single phase model.
- The study can be extended for turbulent flow using different fluids and different thermal boundary conditions.

# REFERENCES


[1] Addini, M. M., and Nassab, A. G., "Combined mixed convection and radiation simulation of inclined lid-driven cavity", Energy Equipment and System, Vol. 6, No. 3, pp. (261-277), 2018.

[2] Al-Amiri, A. M., Khanafer, K. M., and Pop, I., "Numerical simulation of combined thermal and mass transfer in a square lid-driven cavity", International Journal of Thermal Sciences, Vol. 46, pp. (662-671), 2007.

[3] Afrouzi, H., and Farhadi, M., "Mixed convection heat transfer in a lid-driven enclosure filled by nanofluid", Iranica Journal of Energy and Environment, Vol. 4(4), pp. (376-384), 2013.

[4] Belmiloud, M. A., and Chemloud, N. E. S., "Numerical study of mixed convection coupled to radiation in a square cavity with lid-driven", International Journal of Aerospace and Mechanical Engineering, Vol. 9, No. 10, 2015.

[5] Biswas, N., Mannan, N. K., and Mahapatra, P. S., "Enhanced thermal energy transport using adiabatic block inside lid-driven cavity", Internalional Journal of Heat and Mass Transfer, Vol. 100, pp. (407-427), 2016.

[6] Bakar, N. A., Roslan, R., Karimipour, A., and Hashim, I., "Mixed convection in lid-driven cavity with inclined magnetic field", Sains Malaysiana, Vol. 48(2), pp. (451-471), 2019.

[7] Balootaki, A. A., Karimipour, A., and Toghraie, "Nano scale lattice Boltzmann method to simulate the mixed convection heat transfer of air in a lid-driven cavity with an endothermic obstacle inside", Vol. 508, pp. (681-701), 2018.

[8] Bhoite, M.T., Narasimham, G.S.V.L., and Murthy, M.V.K., "Mixed convection in a shallow enclosure with a series of heat generating components", International Journal of Thermal Sciences, Vol. 44, pp. (125-135), 2005.

[9] Chamkha, A. J., "Hydromagnetic combined flow in a vertical lid-driven cavity with internal heat generation or absorption", Numerical Heat Transfer, Vol. 41, pp. (529-546), 2002.

[10] Cheng, T. S., and Liu, W. H., "Effect of cavity inclination on mixed convection heat transfer in a lid-driven cavity flows", Computers and Fluids, Vol. 100, pp. (108-122), 2014.

[11] Chowdhury, K., Alim, A., and Hossen, M., "Natural convection in a partially heated and cooled square enclosure containing a diamond shaped heated block", International Journal of Fluid Mechanics and Thermal Sciencs, Vol. 6, Issue. 1, pp. (1-8), 2020.

[12] Deb, D., Poudel, S., and Chakrabarti, A., "Numerical simulation of hydromagnetic convection in a lid-driven cavity containing a heat conducting inclined elliptical obstacle with joule heating", International Journal of Engineering Research and Technology, Vol. 6, Issue. 10, pp. (177-185), 2017.

[13] Esfe, M. H., Esforjani, M. S. S., and Akbari, M., "Mixed convection flow and heat transfer in a lid-driven cavity subjected to nanofluid: Effect of temperature concentration and cavity inclination angles", Heat Transfer Research, Vol. 45(5), pp. (453-470), 2014.

[14] Esfe, M. H., Ghadi, A. Z., and Norrozi, M. J., "Numerical simulation of mixed convection within Nanofluid filled cavities with two adjacent moving walls", Transactions of the Canadian Society for Mechanical Engineering, Vol. 37, No. 4, pp. (1073-1083), 2013.

[15] Farid, S. K., Billah, M. M., Rahman, M. M., and Sharif, U. M., "Numerical study of fluid flow on magneto-hydrodynamic mixed convection in a lid driven cavity having a heated circular hollow cylinder", Procedia Engineering, Vol: 56, pp. (474-479), 2013.

[16] Geridonmez, B. P., and Oztop, H. F., "Mixed convection heat transfer in a lid-driven cavity under the effect of partial magnetic field", Heat Transfer Engineering, Vol. 42, Issue. 10, pp. (875-887), 2021.

[17] Guimaraes, P. M., and Menon, G. J., "Natural nanofluid-based cooling of a protuberant heat source in a partially cooled enclosure", International Communications in Heat and Mass Transfer, Vol. 45, pp. (23-31), 2013.

[18] Ismael, M.A., "Numerical solution of mixed convection in a lid-driven cavity with arc-shaped moving wall", Engineering Computations, Vol. 34, pp. (869–891), 2017.

[19] Ismael, M.A., Pop, I., and Chamkha, A.J., "Mixed convection in a lid-driven square cavity with partial slip", International Journal of Thermal Science, Vol. 82, pp. (47–61), 2014.

[20] Khanafer, K. M., Al-Amiri, A. M., and Pop, I., "Numerical simulation of unsteady mixed convection in a driven cavity using an externally excited sliding lid", European Journal of Mechanics B/Fluids, Vol. 26, pp. (669-687), 2007.

[21] Kahveci, K., "Natural convection in a partitioned vertical enclosure heated with a uniform heat flux", Journal of Heat Transfer, Vol. 129, pp. (717-726), 2007.

[22] Luo, W. J., and Yang, R. J., "Multiple fluid flow and heat transfer soluitions in a two-sided lid-driven cavity", International Journal of Heat and Mass Transfer, Vol. 50, pp. (2394-2405), 2007.

[23] Moallemi, M.K., and Jang, K.S., "Prandtl number effects on laminar mixed convection heat transfer in a lid-driven cavity", International Journal of Heat and Mass Transfer, Vol. 35, pp. (1881–1892), 1992.

[24] Mansour, N. B., Ben-Cheikh, N., Ben-Beya, B., and Lili, T., "Mixed convection of heat transfer in a square lid-driven cavity", International Letters of Chemistry, Physics and Astronomy, Vol. 55, pp. (180-186), 2015.

[25] Munshi, M. J. H., Alim, M. A., and Mostafa ,G., "A numerical study of mixed convection in square lid-driven with internal elliptic body and constant flux heat source on the bottom wall", International Journal of Engineering and Applied Sciences, Vol. 2, Issue. 6, pp. (42-49), 2016.

[26] Munshi, M. J. H., and Alim, M. A., "Effect of hydromagnetic mixed convection double lid-driven square cavity with inside elliptic heated block", Journal of Scientific Research, Vol. 9(1), pp. (1-11), 2016.

[27] Malik, S., and Nayak, A. K., "A comparative study of mixed convection and its effect on partially active thermal zones in a two sided lid-driven cavity filled with nanofluid", Engineering Science and Technology, an International Journal, Vol. 19, pp. (1283-1298), 2016.

[28] Nada, E. A., and Chamkha, A. J., "Mixed convection flow of a nanofluid in a lid-driven cavity with a wavy wall", International Communications in Heat and Mass Transfer, Vol. 57, pp. (36-47), 2014.

[29] Oztop, H. F., and Dagtekin, I., "Mixed convection in two-sided lid-driven differentially heated square cavity", International Journal of Heat and Mass Transfer, Vol. 47, pp. (1761-1769), 2004.

[30] Oztop, H. F., Zhao, Z. and Yu, B., "Fluid flow due to combined convection in lid-driven enclosure having a circular body", International Journal of Heat and Fluid flow, Vol. 30, pp. (886-901), 2009.

[31] Oztop, H.F., Al-Salem, K., and Pop, I., "MHD mixed convection in a lid-driven cavity with corner heater", International Journal of Heat and Mass Transfer, Vol. 54, pp. (3494–3504), 2011.

[32] Oztop, H. F., Sakhrich, A., Nada, E. A., and Salem, K. A., "Mixed convection of MHD flow in nano-fluid filled and partially heated wavy walled lid-driven enclosure", International Communications in Heat and Mass Transfer, Vol. 86, pp. (42-51), 2017.

[33] Omari, R., "Numerical investigation of mixed convection flow in a lid-driven cavity", American Journal of Computational Mathematics, Vol. 6, No. 3, pp. (251-258), 2016.

[34] Ogut, E. B., “Magnetohydrodynamic mixed convection in a lid-driven rectangular enclosure partially heated at the bottom and cooled at the top”, Thermal Science, Vol. 21, Issue. 2, pp. (863-874), 2017.

[35] Parvin, S., Siddiqua, A., and Elias, M., “Effect of Reynold’s number for mixed convection flow of nanofluid in a double lid-driven cavity with heat generating obstacle”, Heat and Mass Transfer Research Journal, Vol. 1, No. 1, pp. (79-87), 2017.

[36] Rahman, M. M., Alim, M. A., and Chowdhury, M. K., “Magnetohydrodynamic mixed convection around a heat conducting horizontal circular cylinder in a rectangular lid-driven cavity with joule heating”, Journal of Scientific Research, Vol. 1, No. 3, pp. (461-472), 2009.

[37] Rahman, M. M., Oztop, H. F., Mekhilef, S., Saidur, R., Ahsan, A., and Al-Salem, K., “Modeling of unsteady natural convection for double-pipe in a partially cooled enclosure”, Numerical Heat Transfer, Part: A Applications, Vol. 66, Issue. 5, pp. (582-603), 2014.

[38] Saha, L. K., Somaddar, M. C., and Uddin, K. M. S., “Mixed convection heat transfer in a lid-driven cavity with wavy bottom surface”, American Journal of Applied Mathematics, Vol. 1(5), pp. (92-101), 2013.

[39] Sharif, M. A. R., “Laminar mixed convection in shallow inclined driven cavities with hot moving lid on top and cooled from bottom”, Applied Thermal Engineering, Vol. 27, pp. (1036-1042), 2007.

[40] Sivasankaran, S., Malleswaran, A., Bhuvaneswari, M., and Poo, B. G., “Hydro-magnetic mixed convection in a lid-driven cavity with partially thermally active walls”, Scientia Tranica, Vol. 24(1), pp. (153-163), 2017.

[41] Wu, F., Wang, G., and Zhou, W., “A thermal Nonequilibrium approach to natural convection in a square enclosure due to the partially cooled sidewalls of the enclosure”, Numerical Heat Transfer, Vol. 67, Issue. 7, pp. (771-790), 2015.

[42] Yapici, K., and Obut, S., “Laminar mixed convection heat transfer in a lid-driven cavity with modified heated wall”, Heat Transfer Engineering, Vol. 36, No. 3, pp. (303-314), 2015.